Journal of Earth Science, *Vol. 29*, *No. 3*, *p. 537–555*, *June 2018* *ISSN 1674-487X*
Printed in China
https://doi.org/10.1007/s12583-017-0974-7

A newly Found Biotite Syenogranite in the Huangshaping Polymetallic Deposit, South China: Insights into Cu Mineralization

Weicheng Jiang[1], **Huan Li**[*2], **Jinghua Wu**[1], **Zhekai Zhou**[1], **Hua Kong**[2], **Jingya Cao**[3]

1. *Faculty of Earth Resources*, *State Key Laboratory of Geological Processes and Mineral Resources*, *China University of Geosciences*, *Wuhan* 430074, *China*
2. *Key Laboratory of Metallogenic Prediction of Nonferrous Metals and Geological Environment Monitoring*, *Ministry of Education*, *School of Geosciences and Info-Physics*, *Central South University*, *Changsha* 410083, *China*
3. *CAS Key Laboratory of Crust-Mantle Materials and Environments*, *School of Earth and Space Sciences*, *University of Science and Technology of China*, *Hefei* 230026, *China*

Weicheng Jiang: https://orcid.org/0000-0003-2939-2231; Huan Li: https://orcid.org/0000-0001-5211-8324

ABSTRACT: The W-Sn-Mo-Cu-Pb-Zn polymetallic mineralization in the Huangshaping Deposit is associated with different types of Jurassic granitic intrusions such as quartz porphyry, granophyre and granite porphyry. In this study, we carried out detailed mineralogical, petrological, geochemical, zircon U-Pb geochronological and Hf isotopic studies on a newly found, Cu-mineralization-related fine-grained biotite syenogranite at Huangshaping. This syenogranite is mainly composed of quartz (40%), K-feldspar (30%), plagioclase (15%) and biotite (5%), enriching in SiO_2 (75.58 wt.%–76.02 wt.%), K_2O (5.24 wt.%–5.78 wt.%), Al_2O_3 (12.23 wt.%–12.46 wt.%), Rb (405 ppm–504 ppm), U (18.5 ppm–40.7 ppm), Th (47 ppm–52.3 ppm), Nb (49.6 ppm–57.5 ppm), and Cu (54 ppm–288 ppm) whereas depleting in P_2O_5 (0.01 wt.%), TiO_2 (0.05 wt.%–0.06 wt.%), Ba (5 ppm–13.1 ppm), Sr (6.8 ppm–23.9 ppm) and Eu (0.04 ppm–0.05 ppm), with A_1-type alkaline granite characteristics. Magmatic and hydrothermal zircons were separated from a Cu-mineralized syenogranite sample and yielded the $^{206}Pb/^{238}U$ concordant ages of 156.5±1.8 and 154.4±2.9 Ma, representing the intrusive age of the pluton and probable Cu-mineralization time at the Huangshaping Deposit, respectively. Zircon Hf isotopes suggest a crust-derived (partial melting of Paleoproterozoic basement) magma for the syenogranite, with some degree of crust-mantle interaction. We infer that the syenogranite is a transitional phase between the granophyre and the granite porphyry, not only contributed greatly to the Cu mineralization but also provided W-Sn polymetallic ore-forming metals for the Huangshaping Deposit.

KEY WORDS: zircon U-Pb dating, Hf isotope, A-type granite, southern Hunan.

0 INTRODUCTION

The Huangshaping W-Sn-Mo-Cu-Pb-Zn polymetallic deposit is located in the central Nanling Range, severing as the largest lead-zinc production base in the Hunan Province, South China (Xu et al., 2007). The polymetallic mineralization has been proven to be related to three types of granites, including quartz porphyry, granophyre and granite porphyry. In pace with the continuous exploration in recent years, increasing Cu polymetallic ore bodies have been discovered, showing good prospecting prospect at depth (Lei et al., 2010). However, the origin of the Cu mineralization is still controversial (Li et al., 2014a, b; Wang et al., 2011; Zeng, 2001; Zhong, 1996). Previous studies pointed out that the Cu mineralization is related to the quartz porphyry, evidenced by the sporadic Cu mineralization hosted in the quartz porphyry bodies (Li et al., 2014a, b). In contrast, Pb-Zn mineralization is considered to be generated by granophyre, and granite porphyry is closely associated with the W-Sn-Mo-Fe mineralization (Ding et al., 2016a; Li et al., 2014a, b; Yuan et al., 2014; Zhu et al., 2012; Wang et al., 2011; Zhong, 1996; Tong, 1986). These inferences were further illustrated by the whole-rock geochemical studies on the granites, which showed that concentrations of some ore-forming elements such as Pb, Zn are in the same level among three types of granites, while Cu is considerably enriched in quartz porphyry and W-Sn are mostly concentrated in granite porphyry (Li et al., 2014b; Qi et al., 2012; Quan et al., 2012; Liu et al., 2009; Yao et al., 2005). Though the corresponding relations between the granite and mineralization types were determined based on factual basis, the magmatic evolutionary processes and their bearings on different types of mineralization are increasingly questioned by the recent studies (Ding et al., 2016a, b; Li et al., 2014a, b). The latest-

*Corresponding author: lihuan@csu.edu.cn

Manuscript received July 30, 2017.
Manuscript accepted December 20, 2017.

prospected Cu ores are found much deeper than the intrusive depth of the quartz porphyry, thus the source of Cu at the Huangshaping Deposit is still unclear.

Recently, a new type of granite, biotite syenogranite, has been revealed to be spatially associated with the deep Cu ore bodies by the systematic drilling work. In this contribution, analysis on petrology, whole-rock major-trace element geochemistry, zircon U-Pb chronology and Hf isotope of the syenogranite has been conducted in comparison with those of quartz porphyry, granophyre and granite porphyry from previous studies. We are aiming to reveal the genesis of this new type granitoid and provide some insights into the origin of the Cu-polymetallic mineralization in the Huangshaping Deposit.

1 REGIONAL AND DEPOSIT GEOLOGY

The Nanling Range is located in the central part of the South China Block, geographically including southern Jiangxi, southern Hunan and northern Guangdong and eastern Guangxi (Fig. 1a). It is the largest W-Sn polymetallic ore province in China and even in the world (Mao et al., 2007). In the southern Hunan Province (central part of Nanling region), abundant Jurassic granitic plutons (e.g., Qianlishan and Qitianling) intruded along the Chenzhou-Linwu deep fault, forming a regional magmatic-tectonic belt (Fig. 1b). The granite-associated W-Sn polymetallic deposits are represented by Xianghualing, Shizhuyuan, Huangshaping, Xintianling and Yaogangxian in the region (Tong et al., 2000).

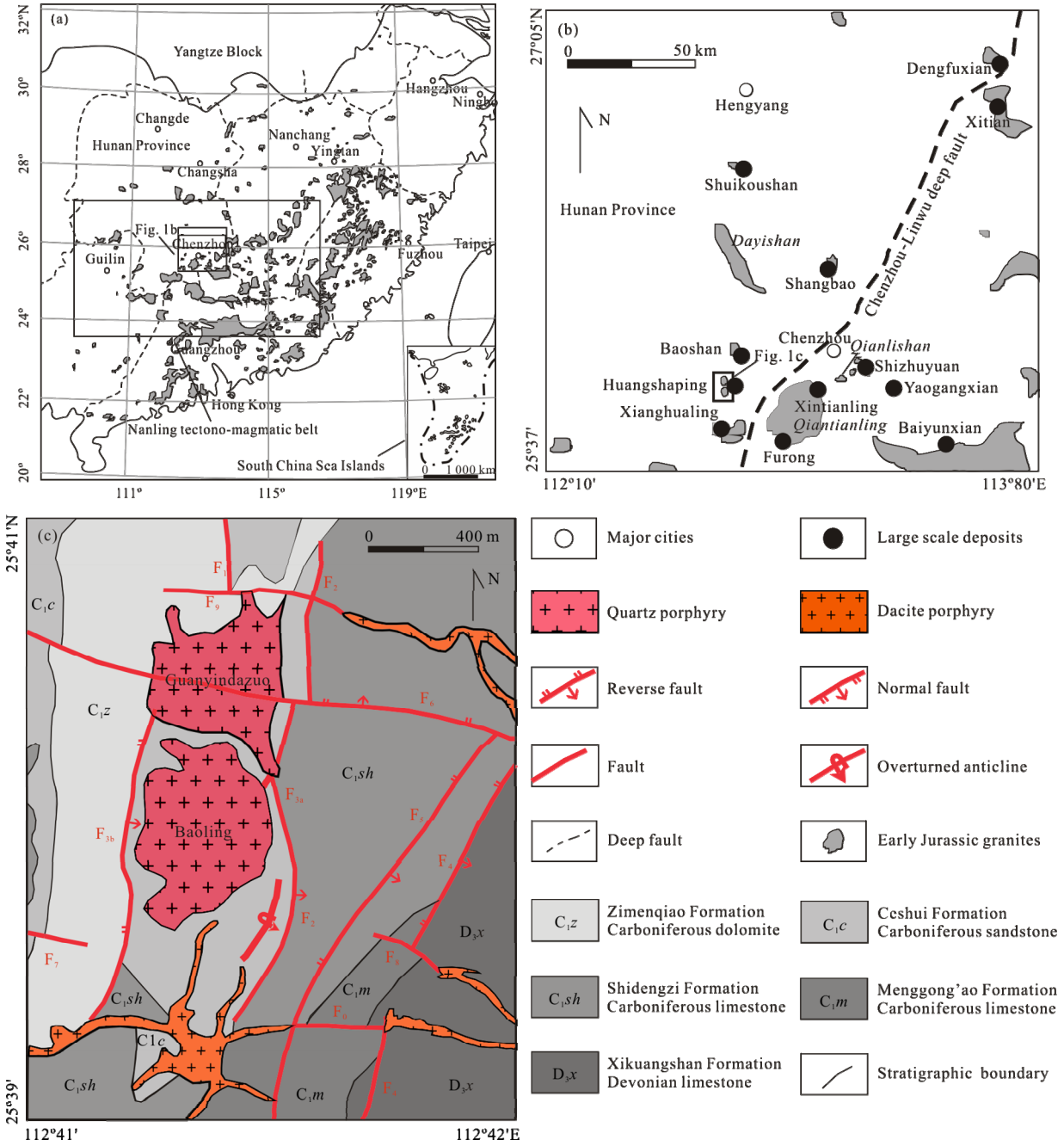

Figure 1. (a) Sketch geological map of South China (after http://bzdt.nasg.gov.cn/, No. GS(2016)1597), showing the distribution of Early Jurassic magmatic rocks; (b) regional geological map of southern Hunan; and (c) sketch geological map of the Huangshaping Deposit (modified from Li et al., 2014a, b).

In the Huangshaping area, the outcropping strata are relatively simple, including Upper Devonian Shetianqiao Formation and Xikuangshan Formation, and Lower Carboniferous Ceshui Formation, Menggong'ao Formation, Shidengzi Formation and Zimenqiao Formation (Fig. 1c; Wang et al., 2011; Yao et al., 2007). Lithology of these strata mainly contains limestone, dolomitic limestone, calcareous sandstone, bioclastic limestone and sand-shale. The most advantageous ore-bearing wall-rock is Shidengzi Formation limestone; and Ceshui Formation sandstone is the secondary ore-bearing stratum which also served as a significant shelter layer for the mineralization at the Huangshaping Deposit (Lei et al., 2010).

The tectonic framework of the Huangshaping Deposit consists of a series of nearly SN-striking reversed faults (F_1, F_2, F_3) and overturned anticlines, coupled with three groups of EW-striking faults (F_0, F_6 and F_9). As the foremost ore-control structures, these faults and folds in the two directions not only provided a well-shaped trap space for the mineralization but also dominated the emplacement of various granitic plutons (Ma et al., 2007).

Extensive and frequent magmatism resulted in the intrusions of various granitic plutons at the Huangshaping area. Among them, the quartz porphyry and dacite porphyry are exposed to the surface (Fig. 1c), while granite porphyry and granophyre are completely concealed for hundreds of meters beneath the surface (Fig. 2a). These four types of granitoids all belong to Jurassic hypabyss intrusions with a variable intrusive time span ranging of 180–150 Ma (Ding et al., 2016b; Li et al., 2014a; Yuan et al., 2014; Ai, 2013; Quan et al., 2012; Wang et al., 2011; Lei et al., 2010; Yao et al., 2005). With a dumbbell shape, the quartz porphyry is situated in the middle part of the Huangshaping area (Zhong, 1996). The concealed tongue-shaped granophyre intruded in footwall of the fault F_1 (Li et al., 2014a, b). Occurring in the southeast portion of the Huangshaping area, the concealed granite porphyry is located between the faults F_1 and F_2 and has the largest intrusive volume (Li et al., 2014a, b; Yuan et al., 2014; Zhong, 1996). The newly found syenogranite was revealed beneath the granophyre in the northern portion of the deposit, probably with a smallest intrusive scale (Fig. 2b).

In the Huangshaping Deposit, hundreds of hydrothermal filling replacement-type Pb-Zn and dozens of skarn-type W-Mo-Bi-Sn-Fe ore bodies were discovered during past exploration activities (Chen et al., 2013). The former is mainly distributed along the contact zone between limestone and granophyre, and the latter occurs in massive skarns around the concealed granite porphyry. These ore bodies are in different sizes, ranging from 800 to 1 000 m in length, 60 to 400 m in width and 1 to 310 m in thickness. Ore bodies are complicated in morphology, showing vein, crescent, lentoid, irregular, stratoid and columnar shapes. Ore minerals are mostly composed of sphalerite, chalcopyrite, galena and pyrite for the Pb-Zn ores, and magnetite, scheelite, molybdenite and bismuthinite for the W-Mo-Bi-Sn-Fe ores (Chen et al., 2013). Four types of Cu ore bodies have been differentiated (Wang et al., 2011): (1) skarn-type distributed around the granite porphyry, (2) hydrothermal filling-replacement-type located close to the granophyre and partially hosted in the syenogranite, (3) stratoid-type existed in the Ceshui Formation, and (4) fine disseminated porphyry-type hosted in the quartz porphyry. Recent exploration revealed that the second type Cu ore bodies with high grade, bulk mass and deep burial depth possess the greatest prospecting potential for Cu resources. Additionally, strong wall-rock alterations such as silicification, K-feldspathization, propylitization, marbleization, muscovitization and biotitization were closely related to the Cu mineralization.

The syenogranite is flesh red-colored with euhedral-subhedral granular texture and massive structure (Fig. 3a). The main rock-forming minerals are fine-grained (0.5–2 mm) and mainly composed of quartz (40%), K-feldspar (30%), plagioclase (15%) and biotite (5%) (Fig. 3b). Among them, plagioclase possesses the best automorphic degree, followed by K-feldspar and quartz. In addition, a small amount of K-feldspar occurs as Carlsbad twin whereas plagioclase is commonly found in polysynthetic twin. The biotite is characterized by relatively large granularity and good automorphic extent. The accessory minerals are mainly composed of zircon and chalcopyrite. Moreover, the syenogranite is locally interspersed by thin chalcopyrite-quartz veins (Fig. 3c), in which sphalerite and pyrite were partly replaced by chalcopyrite (Fig. 3d).

2 SAMPLING AND ANALYTICAL METHODS

Five syenogranite samples were collected at 160–240 m depth of No. ZK1301 drill hole which was arranged at the No. 13 exploration line, No. 56 m level at the Huangshaping Deposit. Thus, the freshness of these samples is fully guaranteed. After sampling, each sample was cut and polished into thin sections and then was crushed by a hammer. Subsequently, a vibration agate mill was used to grind the crushed samples into 200-mesh size.

The measurement of major elements was performed using X-ray fluorescence spectrometry (XRF) at Kyushu University (Japan). Standard sample JA-3 was used to evaluate accuracy, and the results show that the experimental error was less than 5%. Trace elements encompassing rare earth elements (REE) were determined by inductively coupled plasma mass spectrometry (ICP-MS) at the ALS Laboratory in Canada. Ascertained by the analysis of standard sample JG-2, the experimental error of most trace elements was less than 10%.

Zircon crystals were separated from a mineralized syenogranite sample (HSP-2) by using standard techniques: hand-picked to purify zircon crystals under binocular microscope→ mounted in epoxy resin→polished to expose the grain center. Cathodoluminescence (CL) imaging was implemented by scanning electron microscope (SEM) equipped with an energy dispersive spectroscopy (EDS) system and a CL3+ detector under an operating condition at 15 kV and 20 nA at the Beijing Geo-Analysis Co. Ltd. Zircon U-Pb dating and trace element analyses were conducted by LA-ICP-MS at Beijing Geo-Analysis Co. Ltd., using a GeoLas 2005 excimer laser ablation system that coupled to an Agilent 7500a ICP-MS. For the instrument, laser energy and frequency were 70 mJ and 8 Hz, respectively; spot size and ablated depth were 32 and 20–40 μm, respectively. During the experimental process, helium acted as a carrier gas whereas argon was used as the make-up and the mixture gas in carrier gas. In order to improve precision and reduce detection limit for the analysis, nitrogen was added into central gas stream

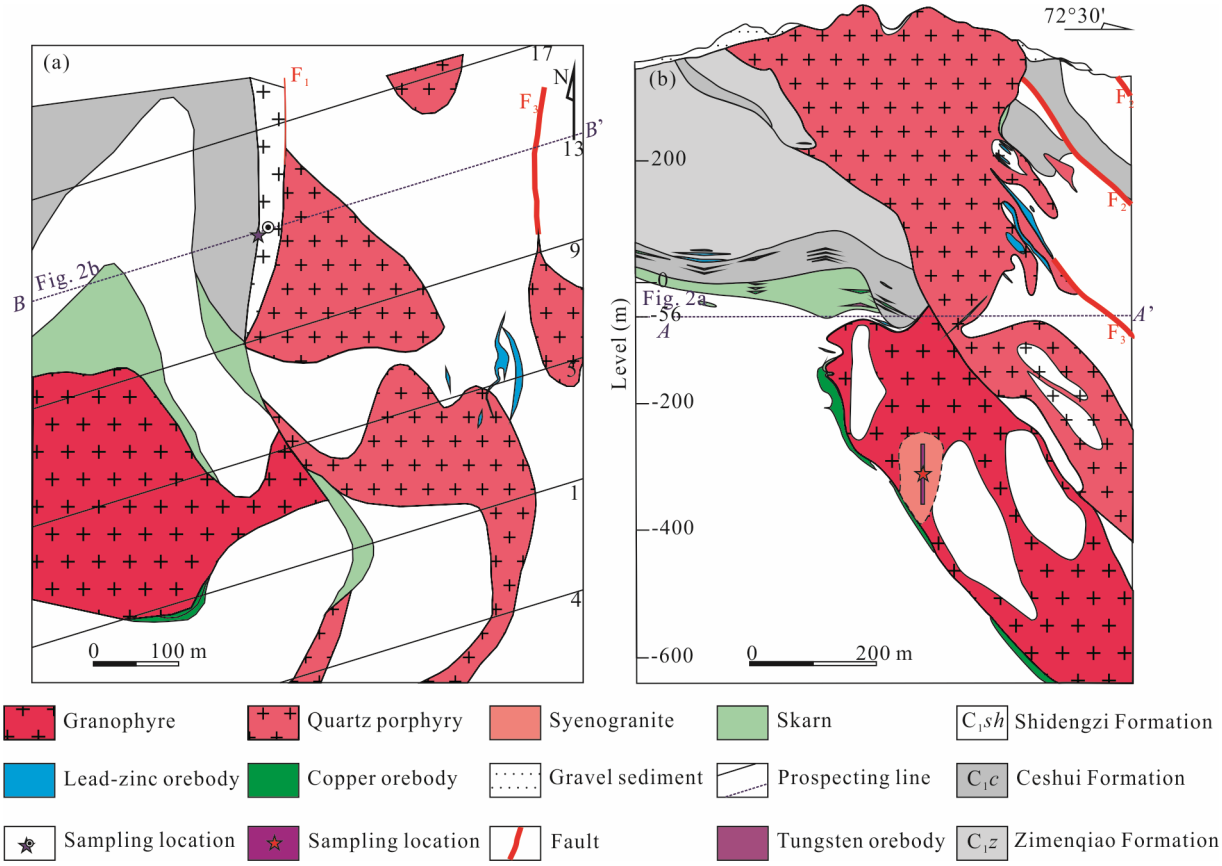

Figure 2. (a) Geological map of 56 m level and (b) cross-section of No. 13 exploration line in the Huangshaping Deposit (after Wang et al., 2011). The newly found syenogranite is located in the northern portion of the deposit, beneath the granophyre body without absolute boundaries (noted by dotted lines in Fig. 2b).

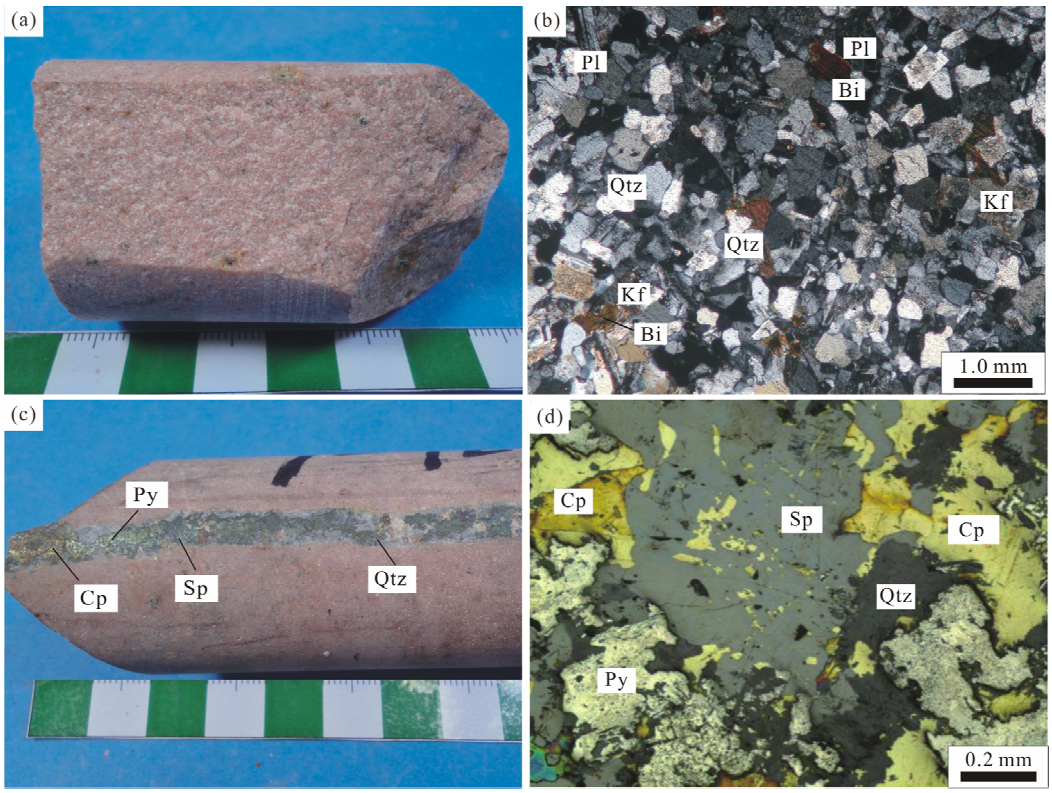

Figure 3. Hand specimens of the syenogranite (a), photomicrographs of the syenogranite (b), quartz-chalcopyrite veins in the syenogranite (c), typical Cu-ores related to the syenogranite (d). Py. Pyrite; Cp. chalcopyrite; Sp. sphalerite; Qtz. quartz; Pl. plagioclase; Kf. K-feldspar; Bi. biotite.

(Ar+He) of the Ar plasma (Liu et al., 2010; Hu et al., 2008). Each analysis contained a background acquisition of approximately 20–30 s (gas blank) followed by 50 s of data acquisition from the sample. Zircon 91500 is the external standard for U-Pb dating which was analyzed twice every 5 samples. As the other standard sample, zircon standard GJ-1 was analyzed as an unknown. The weighted mean $^{206}Pb/^{238}U$ age for GJ-1 is 597.51± 5.26 Ma (2σ, n=10), which corresponds to the recommended values within uncertainty (599.81±1.7 Ma, 2σ) (Jackson et al., 2004). Time-dependent drifts of U-Th-Pb isotopic ratios were calibrated using a linear interpolation (with time) for every five analyses under variations in the 91500 standard. Preferred U-Th-Pb isotopic ratios used for 91500 were referenced from Wiedenbeck et al. (2004). Additionally, NIST SRM 610 was analyzed every 10 samples to make a correlation of time-dependent drift of sensitivity and mass discrimination in trace element results. Trace element compositions of zircons were calibrated by internal standardization (^{29}Si, assumed 32.7 wt.% SiO_2 for zircon unknowns). Detailed experimental methods and conditions for LA-ICP-MS trace element analyses were introduced in Liu et al. (2008) and Chen et al. (2011). Off-line background and analytical signals, time-drift correction and quantitative calibration of zircon U-Pb dating and trace element compositions were selected and integrated by ICPMSDataCal 10.1 (Liu et al., 2010). The calibration of common Pb correction based on the method was proposed by Andersen (2002). U-Pb concordia diagrams and weighted mean ages were calculated by Isoplot 4.5 (Ludwig, 2003).

In-situ analysis of zircon Lu-Hf isotopes was tested by laser ablation-multi collector-inductively coupled plasma mass spectrometry (LA-MC-ICP-MS) at Beijing Createch Testing Technology Co. Ltd. In the course of the experiment, helium was applied as the carrier gas of denudation material, and the diameter of denudation was 40 μm. The international standard sample GJ-1 of zircon was used as reference material during the determination, and most of the analytical spots are the same as those of U-Pb dating. Related instrument operation conditions and detailed analysis process are described in Wu et al. (2006) and Hou et al. (2007). In the analysis process, the $^{176}Hf/^{177}Hf$ ratios obtained for zircon standard GJ-1 are 0.282 007±0.000 007 (2σ, n=36), which is in good agreement with the reported values (Morel et al., 2008) within the error range.

3 RESULTS

3.1 Major Elements

The analytical results of major element compositions of the syenogranite are presented in Table 1. The loss on ignition (LOI) for each sample is less than 2 wt.%, indicating high reliability of the data. The syenogranite samples have consistent chemical compositions: SiO_2=75.58 wt.%–76.02 wt.% (average=75.76 wt.%), Al_2O_3=12.23 wt.%–12.46 wt.% (average=12.36 wt.%), K_2O=5.24 wt.%–5.78 wt.% (average=5.44 wt.%), Na_2O=2.73 wt.%–3.36 wt.% (average=2.97 wt.%), CaO=0.81 wt.%–1.35 wt.% (average=1.07 wt.%), MgO=0.18 wt.%–0.27 wt.% (average=0.22 wt.%) and FeO_t=0.37 wt.%–1.15 wt.% (average= 0.72 wt.%). Compared to the other granite types at the Huangshaping Deposit, the syenogranite is characterized by high silicon, aluminum and alkalinity (K_2O+Na_2O=8.08 wt.%–8.66 wt.%) (Table 1). The average content of SiO_2 in syenogranite is higher than that in other granite types by 1 wt.%–2 wt.%. The average content of K_2O in syenogranite is only slightly higher than that in granite porphyry and is lower than that in quartz porphyry and granophyre by ~1 wt.%. The average content of Na_2O is gradually increased by the order of quartz porphyry, granophyre, granite porphyry and syenogranite. In addition, the average contents of FeO_t (0.72 wt.%) and MgO (0.22 wt.%) in syenogranite samples are both the minimum quantities among the four types of granites, reflecting a relatively less abundant of mafic minerals in syenogranite. Based on the SiO_2 vs. (K_2O+Na_2O) diagram (Fig. 4a) and microscopic studies (Fig. 3b), the new type granite can be formally classified as fine-grained biotite syenogranite. Furthermore, the syenogranite can be divided into high K calc-alkaline shoshonite granite due to its low Rittmann indexes (2–3) whereas high K_2O compositions (Fig. 4b). In addition, the syenogranite can be classified as metaluminous to peraluminous granite, similar to other types of granites from the Huangshaping Deposit (Fig. 4c).

3.2 Trace Elements

Trace element compositions (including rare earth elements) of the syenogranite samples are listed in Table 2. Compared to the other granite types in the Huangshaping Deposit, the syenogranite has similar characteristics to quartz porphyry and granophyre in terms of most trace element compositions, such as Cs, Rb, Ta, Zr, Ce, Sm, Gd, Tb, Ho, Dy, Tm and Lu. In contrast, compositions of Ba (average=9.92 ppm), Sr (17.2 ppm), V (<5 ppm) and Eu (average=0.05 ppm) in the syenogranite are close to those of granite porphyry. Moreover, elements such as Ga, Nb, Rb, Ta, U, Y, Sm, Gd, Tb, Er, Tm, Yb and Lu in syenogranite are slightly higher than those of quartz porphyry and granophyre but are comparatively lower than those of granite porphyry, with reverse trends for Ba, Sr, Ce and Eu. For the major ore-forming elements in syenogranite, the average value of Cu (134 ppm) is much higher than that in granophyre (73 ppm) and granite porphyry (1 ppm), and is almost the same as that in quartz porphyry (132 ppm). The average contents of Pb (27 ppm) and Zn (12 ppm) in syenogranite are extremely less than those in quartz porphyry, granophyre and granite porphyry (Table 2). In addition, the average concentration of Mo among the four types of granites shows little difference whereas the As content displays large variations: 120 ppm in granite porphyry, 31 ppm in quartz porphyry, 29 ppm in granophyre and 23 ppm in syenogranite.

On the primitive mantle-normalized multi-elements diagram (Fig. 5a), the four types of Huangshaping granites exhibit strongly negative Ba, Sr, P and Ti anomalies and positive Rb, Th and U anomalies. Overall, more pronounced anomalies are shown for the granite porphyry and syenogranite. The abnormity degrees of Ba, U, Sr and P in the syenogranite are almost the same as those of the granite porphyry, whereas Ti and Rb show significant disparities between the other two types of granites. Additionally, several elements such as Ta, Y, Yb and Lu also act with relatively independent states between granite porphyry and other granites.

The REE distribution curves of all the granite types are generally similar to each other but also show some distinctions (Fig. 5b). Overall, the granite porphyry shows the most significant

Table 1 Major element compositions (wt.%) of syenogranite in the Huangshaping Deposit

Granite type	Syenogranite						Quartz porphyry	Granophyre	Granite porphyry
Sample No.	HSP-1	HSP-2	HSP-3	HSP-4	HSP-5	Average	Average	Average	Average
SiO_2	75.69	76.02	75.72	75.79	75.58	75.76	73.47	74.6	74.91
Al_2O_3	12.46	12.23	12.31	12.4	12.38	12.36	12.16	12.08	12.5
FeO_t	0.37	1.15	0.41	0.86	0.79	0.72	0.94	1.03	1.38
MnO	0.01	0.05	0.01	0.02	0.02	0.02	0.06	0.04	0.08
MgO	0.18	0.19	0.19	0.27	0.27	0.22	0.51	0.49	0.29
CaO	1.21	0.81	1.35	0.99	1.00	1.07	2.02	1.77	1.3
Na_2O	2.88	3.36	3.04	2.84	2.73	2.97	1.74	2.27	2.72
K_2O	5.78	5.24	5.5	5.24	5.46	5.44	6.82	5.84	5.3
TiO_2	0.06	0.06	0.05	0.05	0.06	0.06	0.11	0.1	0.02
P_2O_5	0.01	0.01	0.01	0.01	0.01	0.01	0.02	0.02	0.01
LOI	1.2	0.73	1.2	1.37	1.54	1.21	1.89	1.59	1.29
Total	99.89	99.89	99.89	99.89	99.9	99.89	99.74	99.82	99.8
A/CNK	0.94	0.96	0.92	1.02	1.01	0.97	0.92	0.94	1.01
Na_2O+K_2O	8.66	8.6	8.54	8.08	8.19	8.41	8.56	8.11	8.02

The average data for the quartz porphyry (n=18), granophyre (n=21) and granite porphyry (n=9) are from Li et al. (2014b).

Table 2 Trace and rare earth element compositions (ppm) of syenogranite in the Huangshaping Deposit

Granite type	Syenogranite						Quartz porphyry	Granophyre	Granite porphyry
Sample No.	HSP-1	HSP-2	HSP-3	HSP-4	HSP-5	Average	Average	Average	Average
Ba	5	13.1	10.4	10.7	10.4	9.92	61.42	46.91	7.24
Cr	<10	<10	<10	<10	<10	<10	<10	<10	<10
Cs	16.7	7.59	7.42	12.55	15.75	12	13.46	7.04	17.91
Ga	23.3	22.5	21.8	22.5	23	22.62	19.94	20.8	28.64
Hf	6.9	6.6	7	6	6	6.5	5.71	5.88	8.42
Nb	57.5	55.7	53.2	49.6	53.7	53.94	40.2	43.63	86.02
Rb	500	442	405	468	504	463.8	510.56	425	973.78
Sr	6.8	16.8	16.7	23.9	21.8	17.2	47.07	44.47	13.54
Ta	6.2	5.9	5.8	5.8	5.7	5.88	4.31	4.63	15.12
Th	52.3	50	50.3	48.4	47	49.6	40.72	42.95	46.78
Tl	1.7	1.5	1.2	2.1	2	1.7	2.56	1.91	4.22
U	40.7	20.7	20.5	20.2	18.5	24.12	14.44	15.52	30.09
V	<5	<5	<5	<5	<5	<5	11.1	14.67	<5
Y	62.4	57.3	55.9	55.4	57.5	57.7	40.31	45.26	124.08
Zr	140	130	150	120	120	132	130.56	128.1	106.67
La	21.8	20.8	19.3	19.6	20.6	20.42	23.78	24.15	17.09
Ce	52.3	49.8	46.3	47.1	49.3	48.96	52.9	54.9	44.99
Pr	6.5	6.24	5.68	5.85	6.14	6.08	6.46	6.74	6.18
Nd	24.4	23.4	21.6	21.9	22.8	22.82	24.25	25.36	25.78
Sm	7.35	7.19	6.49	6.74	7	6.95	6.35	6.89	10.63
Eu	0.04	0.05	0.05	0.05	0.05	0.05	0.15	0.14	0.04
Gd	8.78	8.34	8.11	8	8.23	8.29	6.39	7.27	13.66
Tb	1.6	1.5	1.46	1.46	1.47	1.5	1.11	1.27	2.72
Dy	9.97	9.09	9.06	9.05	8.93	9.22	6.74	7.63	17.61
Ho	2.15	1.93	1.96	1.94	1.9	1.98	1.42	1.61	3.8
Er	6.59	5.94	6.02	6.02	5.8	6.07	4.19	4.83	11.95

Table 2 Continued

Granite type	Syenogranite						Quartz porphyry	Granophyre	Granite porphyry
Sample No.	HSP-1	HSP-2	HSP-3	HSP-4	HSP-5	Average	Average	Average	Average
Tm	1.02	0.9	0.94	0.93	0.89	0.94	0.65	0.74	1.95
Yb	6.76	6.06	6.45	6.29	6.23	6.36	4.39	4.97	13.63
Lu	1.01	0.9	0.94	0.92	0.91	0.94	0.67	0.75	2.07
Cu	200	288	55	73	54	134	132	73	1
Zn	10	32	0	0	19	12	91	72	155
Pb	26	45	5	25	33	27	57	65	73
Mo	10	11	9	9	11	10	12	17	17
As	22	4	30	24	33	23	31	29	120
ΣREE	150.27	142.14	134.36	135.85	140.25	140.57	139.46	147.25	172.1
LREE/HREE	2.97	3.1	2.85	2.93	3.08	2.99	4.45	4.07	1.55
$(La/Yb)_N$	2.31	2.46	2.15	2.24	2.37	2.31	3.66	3.29	0.85
Rb/Sr	73.53	26.31	24.25	19.58	23.12	33.36	10.85	9.56	71.89
Ce/Ce*	1.07	1.06	1.07	1.07	1.06	1.07	0.99	1	1.03
Eu/Eu*	0.02	0.02	0.02	0.02	0.02	0.02	0.07	0.06	0.01

The average data for the quartz porphyry (n=18), granophyre (n=21) and granite porphyry (n=9) are from Li et al. (2014b). $Eu/Eu^*=Eu_N/[(Sm_N+Gd_N)/2]$; $Ce/Ce^*=Ce_N/[(La_N^{0.666})\times(Nd_N^{0.333})]$.

negative Eu anomaly, followed by the syenogranite, granophyre and quartz porphyry. The difference of average ΣREE between the syenogranite (140.6 ppm) and the quartz porphyry (139.5 ppm) can be ignored whereas that in the granophyre (147.3 ppm) and the granite porphyry (172.1 ppm) is relatively high. The average LREE/HREE ratios among these granites display an increasing trend from granite porphyry (1.55) to syenogranite (2.99), granophyre (4.07) and then to quartz porphyry (4.55). This difference is manifested by a LREE-enriched pattern for the granite porphyry whereas slightly fractionated REE patterns for the other three types of granites. Furthermore, lanthanide tetrad effects are shown on the REE patterns and are most obvious in the granite porphyry, followed by the syenogranite.

In brief, the syenogranite is characterized by enrichment of LREE, relatively flat HREE patterns and pronounced lanthanide tetrad effect, with a deep "V" shape REE pattern. Additionally, characteristics of trace elements in the syenogranite imply a transitional trend between granite porphyry and the other two kinds of granites (quartz porphyry and granophyre), indicating its own uniqueness.

3.3 Morphology of Zircons

On CL images (Fig. 6), most of the zircon grains separated from the syenogranite possess euhedral-subhedral short angular column characteristics and range from 70 to 150 μm in size, with length/width ratios ranging from 1 : 1 to 2 : 1. Overall, most zircons show oscillatory zoning characteristics with relatively smooth surfaces, suggesting a typical magmatic origin. However, several zircons (represented by Nos. 2, 4, 6, 9, 10, 13, 16, and 20) are characterized by inferior euhedral degree and encircled dark rims, probably indicating a hydrothermal origin. Furthermore, Nos. 7, 12, 14, 17 and 18 zircons show characteristics of moderate roundness and irregular internal texture, implying a detrital origin.

3.4 Zircon Trace Elements

Zircon trace element compositions are shown in Table 3. In most cases, the distinct dark and bright colors in zircons on the CL images can be probably ascribed to different trace element compositions and U/Th ratios. Zircons with oscillatory zoning characteristics (Group 1) have Hf concentrations ranging from 7 672 ppm to 13 276 ppm, Y from 305 ppm to 14 699 ppm, Nb from 0.34 ppm to 336 ppm, Ta from 0.23 ppm to 34.9 ppm, Ti from 1.81 ppm to 35.6 ppm, Pb from 10.1 ppm to 350 ppm, Th from 67.4 ppm to 2 955 ppm and U from 105 ppm to 7 243 ppm. In addition, Group 1 zircons have high U/Th ratios (averaged at 0.8), suggesting a typical magmatic origin. In contrast, dark zircons with irregular shape on CL images (Group 2) possess obviously higher average contents of Hf (14 146 ppm), Y (29 488 ppm), Nb (1 737 ppm), Ta (115 ppm), Ti (130 ppm), Pb (265 ppm), Th (5 448 ppm) and U (10 923 ppm). Moreover, the U/Th ratios (averaged at 0.5) are comparatively lower than those in Group 1 zircons, further indicating their hydrothermal origin.

Two types of REE patterns can be differentiated on the chondrite-normalized diagram (Fig. 7a). Group 1 zircons are characterized by low contents of LREE and significant positive Ce anomalies, showing the characteristics of magmatic zircon. In contrast, Group 2 zircons (Nos. 2, 4, 6, 9, 10, and 20, Fig. 6) possess higher LREE compositions, unobvious Ce anomalies and more pronounced negative Eu anomalies, representing hydrothermal origin. This inference can be further proved by using zircon discrimination diagrams (Figs. 7b, 7c), on which Group 1 zircons mainly plotted in the magmatic field whereas Group 2 zircons plotted in the hydrothermal zircon domain. Thus, we can infer that Group 2 zircons have undergone hydrothermal alteration during postmagmatic stage.

3.5 Zircon U-Pb Ages

Zircon LA-ICP-MS U-Pb dating results are presented in

Table 4 (excluded No. 6 zircon data with a low analytical concordance <90%). The $^{206}Pb/^{238}U$ age data of magmatic zircons and hydrothermal zircons were plotted separately, the obtained concordant ages can represent magma crystallization age and hydrothermal event age (or even mineralization age), respectively (Li et al., 2017a; Li, 2009; Zhang et al., 2009; Hu et al., 2004; Geisler et al., 2003). After removing old inherited zircons (498.1–2 030.3 Ma, Fig. 8a), the $^{206}Pb/^{238}U$ ages of remaining 14 zircons range from 138.2 to 158.2 Ma. Seven magmatic zircons (Group 1) yielded a concordant U-Pb age of 156.5±1.8 Ma (MSWD=0.46, Fig. 8b), representing the crystalizing age of the syenogranite. Another five hydrothermal zircons (Group 2) yielded a concordant U-Pb age of 154.4±2.9 Ma (MSWD=0.25, Fig. 8c). This hydrothermal zircon U-Pb age is consistent with the previous molybdenite Re-Os dating results (ranging from 153.8±4.8 to 159.4±3.3 Ma) at the Huangshaping Deposit (Qi et al., 2012; Lei et al., 2010; Ma et al., 2007; Yao et al., 2007). In addition, the two zircons with ages of 138 Ma (Nos. 16 and 19) have unclear zoning characteristics in CL images and high concordances in U-Pb dating, probably related to a later hydrothermal event.

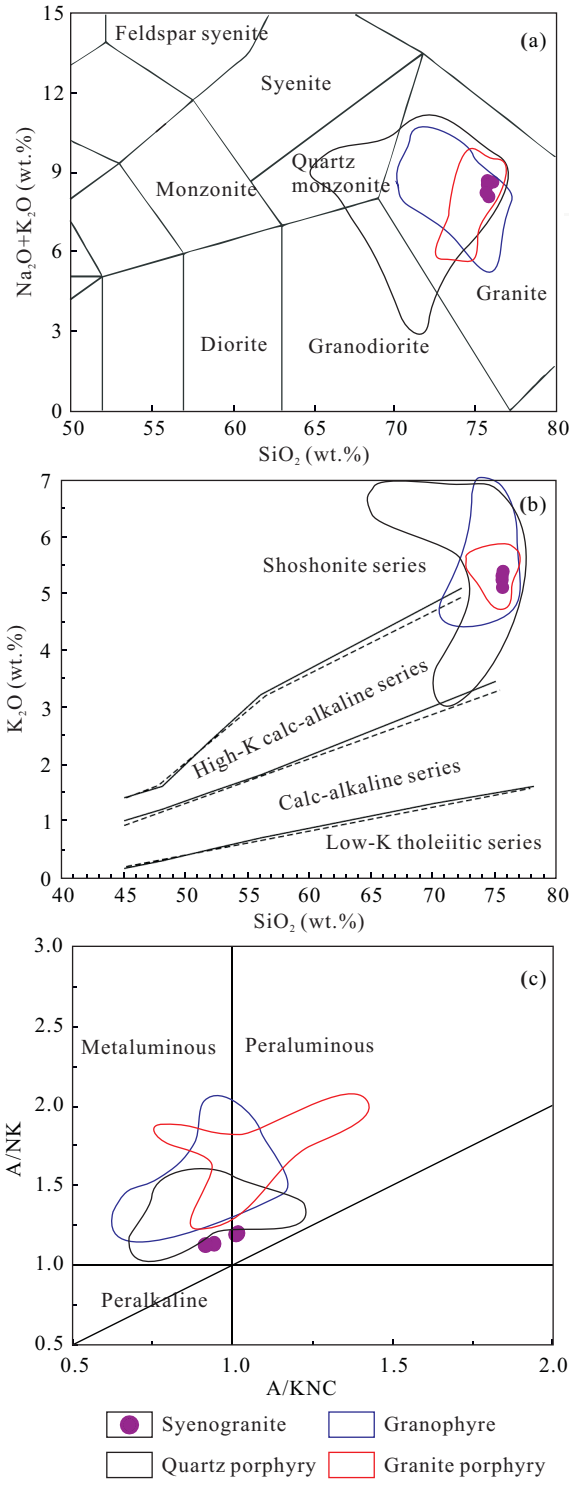

Figure 4. Classification diagrams for granites in the Huangshaping Deposit. (a) SiO_2 vs. (K_2O+Na_2O) diagram (after Le Bas et al., 1986 and Le Maitre, 1989); (b) SiO_2 vs. K_2O diagram (after Wheller et al., 1987); (c) A/KNC vs. A/NK diagram, where A/KNC=Al_2O_3 (molar)/(K_2O+Na_2O+CaO) (molar) and A/NK=Al_2O_3 (molar)/(Na_2O+K_2O) (after Frost et al., 2001). The fields of quartz porphyry, granophyre and granite porphyry are from Li et al. (2014a).

3.6 Hf Isotopes

Zircon Hf isotope analytical results are displayed in Table 5. Since the analytical result of No. 2 spot is abnormal to others, it has been excluded for further discussion. The remaining5 data are divided into two categories: Nos. 1, 3 and 4 are magmatic zircons; Nos. 5 and 6 are inherited zircons. The

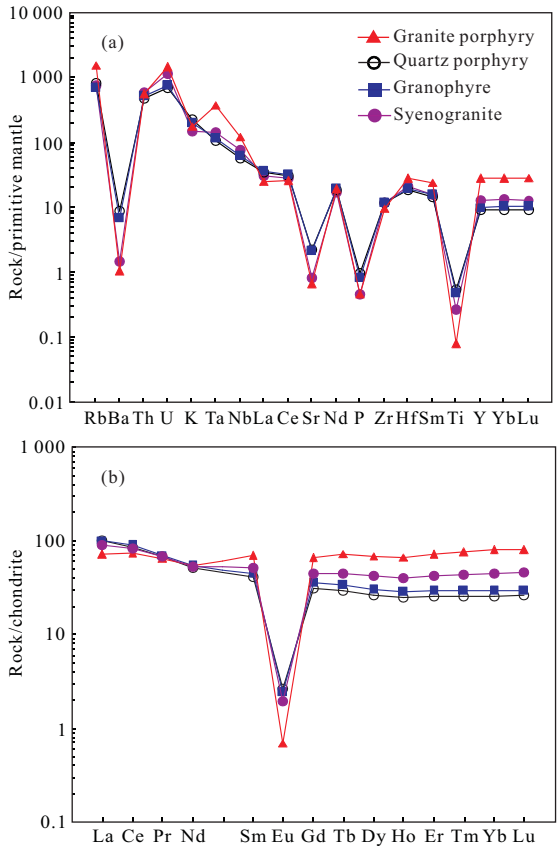

Figure 5. (a) Primitive mantle-normalized trace element, and (b) chondrite-normalized REE patterns for the granites in the Huangshaping Deposit. The average values of quartz porphyry, granophyre and granite porphyry are from Li et al. (2014a). Normalized values for primitive mantle and chondrite are both from Sun and McDonough (1989).

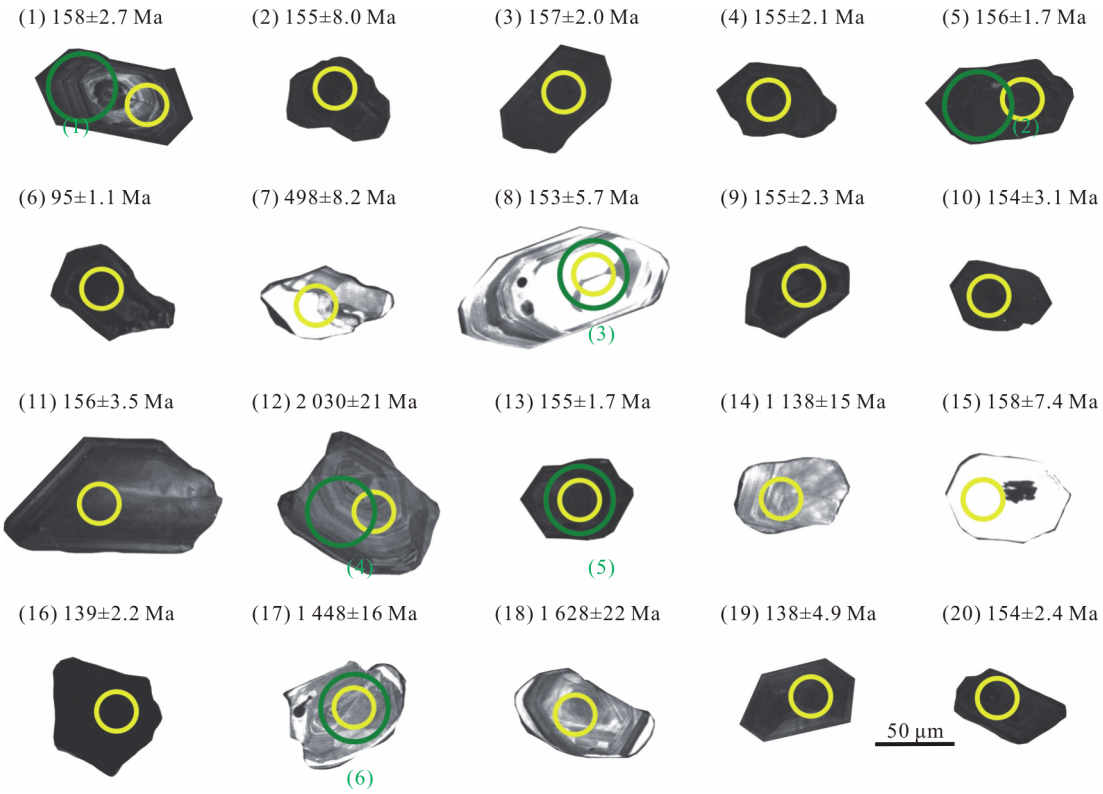

Figure 6. CL-images of analyzed zircons from syenogranite sample HSP-2, showing U-Pb dating (yellow circles) and Hf measuring (green circles) spots.

Table 3 LA-ICP-MS zircon element compositions (ppm) of syenogranite in the Huangshaping Deposit

Spot No.	Hf	Y	Nb	Ta	Ti	Pb	Th	U	Th/U	La	Ce	Pr	Nd	Sm	Eu
HSP-1-01	10 258	2 270	126	11.5	9.31	87	1 057	1 612	0.66	0.50	59.12	0.60	4.28	7.69	1.68
HSP-1-02	19 430	44 626	2 999	317	252	424	11 278	25 415	0.44	24.41	210.37	28.77	156.45	235.71	2.28
HSP-1-03	12 370	6 358	206	28.3	11.2	280	2 955	6 859	0.43	0.56	33.13	0.78	7.13	17.20	0.19
HSP-1-04	13 006	14 893	1 086	27.0	57.8	263	3 511	7 329	0.48	6.63	72.67	7.46	45.05	66.22	0.49
HSP-1-05	12 248	6 463	214	21.6	9.27	254	2 721	6 579	0.41	1.05	29.07	1.20	7.92	18.80	0.12
HSP-1-06	15 434	38 528	2 214	187	167	307	7 033	12 890	0.55	12.3	108	14.8	87.1	171	1.47
HSP-1-07	10 194	305	0.34	0.23	7.89	22.3	67.4	150	0.45	0.02	4.94	0.04	0.02	0.31	0.06
HSP-1-08	10 094	1 249	1.77	0.76	10.7	20.7	277	265	1.05	0.21	26.22	0.13	1.91	3.40	1.10
HSP-1-09	13 490	34 353	2 337	86.4	161	164	4 558	6 872	0.66	17.19	119.71	15.86	90.09	141.13	1.36
HSP-1-10	11 889	33 437	1 373	40.4	119	228	3 782	7 172	0.53	11.08	90.60	11.96	74.38	155.38	1.52
HSP-1-11	9 024	5 744	103	17.1	9.02	122	1 933	1 422	1.36	0.31	58.03	1.14	14.41	28.30	0.88
HSP-1-12	9 688	795	1.56	0.62	9.88	211	184	158	1.16	0.04	26.91	0.19	4.01	6.38	1.60
HSP-1-13	21 064	3 108	157	34.9	8.83	101.7	717	7 243	0.10	1.25	12.05	1.43	8.18	15.97	0.18
HSP-1-14	11 516	963	4.18	2.07	13.2	175	289	331	0.87	0.00	14.77	0.16	1.32	3.72	0.21
HSP-1-15	9 297	652	2.70	0.51	3.75	10.1	102	105	0.97	0.05	38.34	0.09	1.33	2.57	1.35
HSP-1-16	7 672	14 699	336	31.3	35.6	98	2 006	1 820	1.10	2.22	29.07	2.60	23.00	65.97	1.34
HSP-1-17	9 086	2 214	2.53	1.29	8.74	350	406	570	0.71	0.04	9.41	0.30	4.60	8.30	1.24
HSP-1-18	9 144	1 367	1.82	1.06	4.32	216	227	319	0.71	0.18	10.49	0.35	4.45	6.42	0.62
HSP-1-19	13 276	3 797	58.0	11.6	1.81	158	2 594	2 226	1.17	0.22	196.20	0.16	2.34	3.66	0.28
HSP-1-20	11 627	11 089	412	31.2	23.8	204	2 526	5 858	0.43	5.03	50.11	5.09	32.36	53.72	0.48

Table 3 Continued

Spot No.	Gd	Tb	Dy	Ho	Er	Tm	Yb	Lu	ΣREE	LREE	HREE	LREE/HREE	Eu/Eu*	Ce/Ce*
HSP-1-01	38.5	17.5	226	74.0	349	71.1	761	115	1 725.8	73.9	1 651.9	0.04	0.24	22.85
HSP-1-02	878	462	5 607	1 547	6 478	1 196	11 816	1 507	30 148	658.0	29 490	0.02	0.01	1.69
HSP-1-03	102	46.4	609	200	912	181	1 902	279	4 289.7	59.0	4 230.7	0.01	0.01	10.24
HSP-1-04	271	138	1 789	542	2 253	421	4 103	532	10 247	198.5	10 049	0.02	0.01	2.23
HSP-1-05	113	47.5	618	204	938	183	1 961	285	4 407.7	58.2	4 349.6	0.01	0.01	5.58
HSP-1-06	834	441	4 857	1 325	5 206	915	8 846	1 074	23 893	395.39	23 497	0.02	0.01	1.71
HSP-1-07	3.32	1.49	18.1	7.50	47.1	11.6	150	30.2	274.5	5.4	269.2	0.02	0.11	36.06
HSP-1-08	22.3	6.75	92.3	34.9	187	40.8	502	84.8	1 003.3	33.0	970.3	0.03	0.29	38.23
HSP-1-09	620	358	4 790	1 310	5 325	971	9 113	1 043	23 916	385.3	23 530.9	0.02	0.01	1.63
HSP-1-10	728	380	4 733	1 269	4 884	856	7 947	903	22 045	344.9	21 700	0.02	0.01	1.71
HSP-1-11	132	46.8	570	180	778	147	1 472	207	3 636.3	103.1	3 533.2	0.03	0.04	14.18
HSP-1-12	23.1	6.30	72.3	23.8	106	21.2	236	37.4	565.4	39.1	526.3	0.07	0.36	40.61
HSP-1-13	57.2	28.5	348	99.4	464	106	1 459	332	2 932.8	39.1	2 893.7	0.01	0.02	1.94
HSP-1-14	19.9	6.39	84.1	28.8	141	27.1	312	48.0	687.0	20.2	666.8	0.03	0.06	29.27
HSP-1-15	14.9	4.02	52.6	18.7	87.8	17.7	213	36.0	488.1	43.7	444.3	0.10	0.52	108.16
HSP-1-16	369	155	1 765	458	1 741	289	2 679	337	7 917.6	124.2	7 793.4	0.02	0.02	2.58
HSP-1-17	43.7	14.8	193	67.7	329	64.8	688	106	1 530.9	23.9	1 507.1	0.02	0.16	9.32
HSP-1-18	31.9	9.93	123	42.5	197	38.0	403	63.8	931.8	22.5	909.3	0.02	0.11	7.69
HSP-1-19	25.6	11.4	201	93.6	580	141	1 785	302	3 342.3	202.9	3 139.4	0.06	0.06	248.33
HSP-1-20	229	110	1 406	409	1 648	302	2 932	383	7 566.0	146.8	7 419.2	0.02	0.01	2.19

Table 4 LA-ICP-MS zircon U-Pb dating results of syenogranite in the Huangshaping Deposit

Analyzed spot No.	Isotope ratio						Apparent age (Ma)				Con.
	$^{207}Pb/^{206}Pb$	1σ	$^{207}Pb/^{235}U$	1σ	$^{206}Pb/^{238}U$	1σ	$^{207}Pb/^{235}U$	1σ	$^{206}Pb/^{238}U$	1σ	
HSP-1-01	0.050 6	0.002 0	0.173 2	0.006 7	0.024 9	0.000 4	162.2	5.8	158.2	2.7	97%
HSP-1-02	0.053 5	0.006 1	0.184 1	0.022 7	0.024 4	0.001 3	171.6	19.5	155.7	8.0	90%
HSP-1-03	0.051 0	0.002 1	0.174 7	0.006 7	0.024 7	0.000 3	163.5	5.8	157.3	2.0	96%
HSP-1-04	0.047 5	0.001 5	0.160 9	0.005 1	0.024 3	0.000 3	151.5	4.4	154.7	2.1	97%
HSP-1-05	0.046 1	0.001 4	0.157 8	0.004 6	0.024 5	0.000 3	148.8	4.1	156.1	1.7	95%
HSP-1-07	0.053 0	0.002 8	0.589 9	0.031 0	0.080 3	0.001 4	470.8	19.8	498.1	8.2	94%
HSP-1-08	0.031 7	0.006 0	0.171 8	0.017 7	0.024 0	0.000 9	161.0	15.3	153.0	5.7	94%
HSP-1-09	0.065 3	0.003 3	0.181 7	0.014 7	0.023 0	0.001 3	169.6	7.5	155.4	2.3	91%
HSP-1-10	0.051 5	0.002 0	0.173 5	0.006 5	0.024 2	0.000 5	162.4	5.6	154.5	3.1	94%
HSP-1-11	0.053 6	0.003 7	0.181 8	0.012 9	0.024 5	0.000 6	169.6	11.1	156.3	3.5	91%
HSP-1-12	0.123 6	0.003 3	6.403 5	0.181 7	0.370 2	0.004 4	2 032.7	25.0	2 030.3	20.9	99%
HSP-1-13	0.049 9	0.001 2	0.170 3	0.004 5	0.024 4	0.000 3	159.7	3.9	155.4	1.7	97%
HSP-1-14	0.075 7	0.002 2	2.046 5	0.064 5	0.193 1	0.002 8	1 131.1	21.5	1 138.1	15.3	99%
HSP-1-15	0.071 8	0.011 1	0.174 3	0.003 7	0.024 8	0.000 3	315.4	22.9	158.2	7.4	93%
HSP-1-16	0.051 6	0.003 2	0.156 7	0.009 9	0.021 8	0.000 4	147.8	8.7	138.9	2.3	93%
HSP-1-17	0.093 4	0.002 4	3.279 4	0.086 4	0.251 9	0.003 1	1 476.2	20.5	1 448.4	16.2	98%
HSP-1-18	0.098 5	0.002 5	3.933 1	0.109 8	0.287 4	0.004 3	1 620.5	22.6	1 628.6	21.7	99%
HSP-1-19	0.048 0	0.003 1	0.146 0	0.010 5	0.021 7	0.000 8	138.4	9.3	138.2	4.9	99%
HSP-1-20	0.049 2	0.001 5	0.165 3	0.005 6	0.024 1	0.000 4	155.3	4.9	153.8	2.4	98%

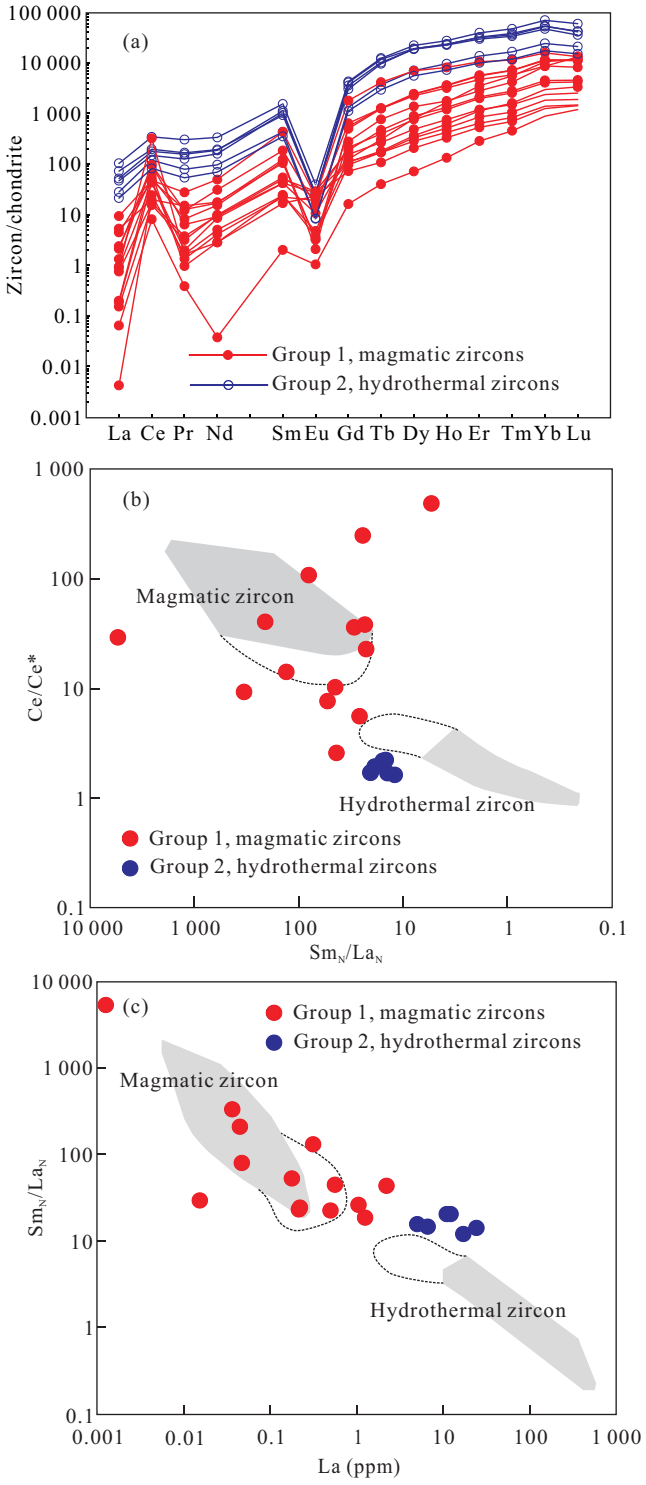

Figure 7. Discriminant diagram of zircon types for the syenogranite in the Huangshaping Deposit. (a) Chondrite-normalized average REE patterns for the syenogranite; (b) Sm_N/La_N vs. Ce/Ce* diagram; (c) La vs. Sm_N/La_N diagram. Normalized values for chondrite are from Sun and McDonough (1989); (b) and (c) after Fu et al. (2009), Hoskin (2005), and Li et al. (2014a).

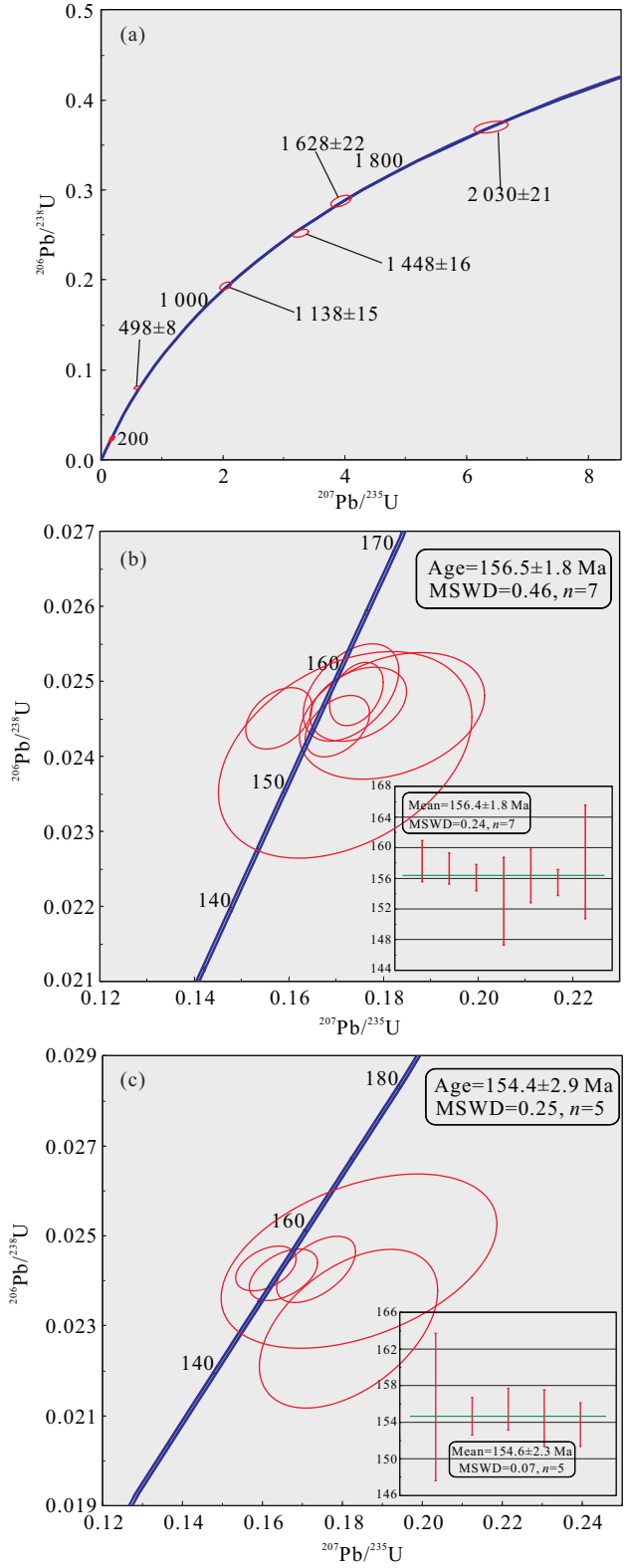

Figure 8. U-Pb concordant ages of (a) all zircons from syenogranite, (b) Group 1 magmatic zircons, and (c) Group 2 hydrothermal zircons.

$^{176}Hf/^{177}Hf$ ratios and $\varepsilon_{Hf}(t)$ values of the magmatic zircons ranging from 0.282 603 to 0.282 390 and from -10.2 to 2.87, respectively, with single-stage Hf model ages (T_{DM1}) of 741–1 206 Ma and two-stage Hf model ages (T_{DM2}) of 1 025–1 850 Ma. On the other hand, the $^{176}Hf/^{177}Hf$ ratios of the inherited zircons range from 0.281 404 to 0.281 713 which are significant lower than those of magmatic zircons. In addition, the $\varepsilon_{Hf}(t)$ values are -6.78 and -3.77 for the inherited zircons, with the T_{DM1} and T_{DM2} ages ranging from 2 188 to 2 550 Ma and from 2 644 to 2 904 Ma, respectively.

4 DISCUSSION

4.1 Timing of Magmatic and Minerogenic Events in Huangshaping

Coupled with the magmatic and hydrothermal zircon dating in this study, the previous zircon U-Pb dating results on different types of granites and molybdenite Re-Os dating on W-Sn polymetallic ores at the Huangshaping Deposit are summarized in Table 6. The variable results on the granites may be ascribed to multiple episodes of magmatism and prolonged magmatic evolution in the deposit area, or could be caused by the dating of samples from distinct magmatic facies from variable sampling locations (Ai, 2013). Thus, it can be concluded that the different ages of crystallization and mineralization are within reasonable error range, further indicating the close genetic relationship between the magmatism and ore formation (Li et al., 2017b; Yuan et al., 2014; Ai, 2013; Yao et al., 2005).

The dating results of the magmatic and hydrothermal event associated with the syenogranite in this study are consistent with the magmatic and ore-forming ages of neighboring world-class W-Sn polymetallic deposits, such as the Shizhuyuan W-Sn-Mo-Bi Deposit, the Yaogangxian W Deposit, the Baoshan Pb-Zn Deposit, the Furong Sn Deposit, the Xianghualing Sn Deposit, the Xintianling W Deposit and the Jinchuantang Sn-Bi Deposit (Table 7). They correspond to the Mesozoic flame up granitic magmatism and polymetallic mineralization in South China (Mao et al., 2013, 2007; Hua et al., 2005).

4.2 Magma Origins: Hf Isotope Implications

Since the close relationship between granitic plutons and ore bodies in the Huangshaping Deposit (Yuan et al., 2014; Lei et al., 2010; Zhong, 1996; Tong, 1986), it is very important to determine the origin of different types of the granites. Although the analytical quantity for Hf isotopes in this study is small, the data are still meaningful in indicating the origin of syenogranite, especially when comparing the data with previous Hf analysis on the various types of granite in the Huangshaping Deposit.

Previous Hf isotopic data on the different types of granites at the Huangshaping Deposit are listed in Table 8. The values of $\varepsilon_{Hf}(t)$ among the granites are generally variable and negative (-19.7 to -0.1) and the two-stage model ages (T_{DM2}) vary from 1 263 to 2 459 Ma, implying that the magmas were mainly derived from Neoarchean–Mesoproterozoic crust but received a certain amount of mantle contribution (Yuan et al., 2014; Ai, 2013; Quan et al., 2012). It is generally accepted that the crust-mantle interaction and mantle contribution in the Nanling region probably have also played an important role in the formation of the world-class polymetallic deposits (Wang et al., 2011; Zhu et al., 2009, 2008; Zhao et al., 2001; Zhou and Li, 2000).

In this study, the $\varepsilon_{Hf}(t)$ values of spots No. 1 and No. 4 are -2.71 and 2.87, respectively, indicating the magma of syenogranite was generated by crust-mantle interaction. The positive $\varepsilon_{Hf}(t)$ value further suggests the participation of mantle material into the syenogranite magma, which is substantially different

Table 5 LA-MC-ICP-MS zircon Lu-Hf isotopic compositions of syenogranite in the Huangshaping Deposit

Spot No.	$^{176}Hf/^{177}Hf$	2σ	$^{176}Lu/^{177}Hf$	2σ	$^{176}Yb/^{177}Hf$	2σ	Age (Ma)	$\varepsilon_{Hf}(t)$	T_{DM1} (Ma)	T_{DM2} (Ma)
HSP-1-1	0.282 603	0.000 019	0.002 087	0.000 100	0.064 903	0.003 070	158.24	-2.71	946	1 382
HSP-1-2	0.283 320	0.000 020	0.006 348	0.000 177	0.238 921	0.005 518	156.08	22.16	-117	-218
HSP-1-3	0.282 390	0.000 024	0.000 614	0.000 005	0.017 832	0.000 278	153.02	-10.20	1 206	1 850
HSP-1-4	0.282 768	0.000 014	0.003 765	0.000 056	0.105 916	0.001 790	155.45	2.87	741	1 025
HSP-1-5	0.281 404	0.000 017	0.000 506	0.000 004	0.015 727	0.000 080	2 030.31	-3.77	2 550	2 904
HSP-1-6	0.281 713	0.000 030	0.001 481	0.000 035	0.039 498	0.001 137	1 448.37	-6.78	2 188	2 644

Table 6 Summary of age dating results for granites and mineralization in the Huangshaping Deposit

Rock type	Mineral	Analytical method	Age (Ma)	Data source
Dacite porphyry	Magmatic zircon	LA-ICP-MS U-Pb	158.5±0.9	Yuan et al. (2014)
Quartz porphyry	Magmatic zircon	SHRIMP U-Pb	152±3.0	Lei et al. (2010)
	Magmatic zircon	LA-ICP-MS U-Pb	155.3±0.7	Ai (2013)
	Magmatic zircon	LA-ICP-MS U-Pb	160.8±1.0	Yuan et al. (2014)
Granophyre	Magmatic zircon	LA-ICP-MS U-Pb	179.9±1.3	Quan et al. (2012)
	Magmatic zircon	LA-ICP-MS U-Pb	150.2±0.4	Ai (2013)
Granite porphyry	Magmatic zircon	LA-ICP-MS U-Pb	161.6±1.1	Yao et al. (2005)
	Magmatic zircon	LA-ICP-MS U-Pb	150.1±0.4	Ai (2013)
	Magmatic zircon	LA-ICP-MS U-Pb	155.2±0.4	Yuan et al. (2014)
Syenogranite	Magmatic zircon	LA-ICP-MS U-Pb	156.5±1.8	This study
	Hydrothermal zircon	LA-ICP-MS U-Pb	154.4±2.9	This study
W-Sn polymetallic ore	Molybdenite	Re-Os isochron	154.8±1.9	Yao et al. (2007)
	Molybdenite	Re-Os isochron	153.8±4.8	Ma et al. (2007)
	Molybdenite	Re-Os isochron	157.5–159.4	Lei et al. (2010)

Table 7 Magmatic and mineralization ages of typical Jurassic granite-related W-Sn polymetallic deposits in the southern Hunan region

Plutons or deposits	Analytical object	Analytical method	Age (Ma)	Data source
Qianlishan granite*	Whole rock	Rb-Sr isochron	152±9	Mao et al. (1995)
	Zircon	SHRIMP U-Pb	152±2	Li et al. (2004)
Shizhuyuan Deposit*	Garnet-fluorite-wolframite	Sm-Nd isochron	149±2	Li et al. (2004)
	Molybdenite	Re-Os isochron	151.0±3.5	Li et al. (1996)
Yaogangxian granite	Zircon	SHRIMP U-Pb	155.4–158.4	Li et al. (2011a)
Yaogangxian Deposit	Molybdenite	Re-Os isochron	158–160	Li et al. (2011b)
	Molybdenite	Re-Os isochron	154.9±2.6	Peng et al. (2006)
Baoshan granite	Zircon	LA-ICP-MS U-Pb	156.3–157.1	Mi (2016)
	Zircon	SHRIMP U-Pb	158±2	Lu et al. (2006)
Baoshan Deposit	Pyrite	Rb-Sr isochron	174±7	Yao et al. (2006)
	Molybdenite	Re-Os isochron	160±2	Lu et al. (2006)
Qitianling granite*	biotite	^{40}Ar-^{39}Ar	156.1–157.5	Mao et al. (2004)
	Zircon	SHRIMP U-Pb	146–156	Li et al. (2006)
	Zircon	SHRIMP U-Pb	156.7±1.7	Li et al. (2005)
Furong orefield*	Cassiterite	LA-ICP-MS U-Pb	156.5±4.1	Wang et al. (2014)
	Phlogopite-muscovite	^{40}Ar-^{39}Ar	150.6–159.9	Peng et al. (2007)
Xianghualing granite	Zircon	LA-ICP-MS U-Pb	150.37–151.18	Lai (2014)
	Muscovite	^{40}Ar-^{39}Ar	154.4–161.3	Yuan et al. (2007)
Xianghualing Deposit	Cassiterite	LA-ICP-MS U-Pb	156–157	Yuan et al. (2008)
Xintianling Deposit	Molybdenite	Re-Os isochron	157.2–162.4	Yuan et al. (2012)
	Quartz	Rb-Sr isochron	157.4±3.2	Cai et al. (2008)
Jinchuantang Deposit	Molybdenite	Re-Os isochron	157.2–162.4	Liu et al. (2012)
	Pyrite	Pb-Pb isochron	164±12	Xiao et al. (2003)

The granitic complexes or deposits marked by "*" are considered to have multiple intrusive or mineralization stages. The age data listed in this table are pointed to the most representative stages.

Table 8 LA-MC-ICP-MS zircon Lu–Hf isotopic compositions of granites in the Huangshaping Deposit

Lithology	$^{176}Hf/^{177}Hf$	$\varepsilon_{Hf}(t)$	T_{DM2} (Ma)	Data source
Dacite porphyry	0.282 463–0.282 588	-7.6 to -3.2	1 411–1 691	Yuan et al. (2014)
Quartz porphyry	0.282 494–0.282 585	-6.6 to -3.6	1 437–1 631	Yuan et al. (2014)
	0.282 085–0.282 432	-11.3 to -0.1	1 556–1 879	Ai (2013)
Granophyre	0.282 115–0.282 221	-19.7 to -15.84	2 220–2 459	Quan et al. (2012)
	0.282 526–0.282 588	-5.8 to -3.5	1 263–1 387	Ai (2013)
Granite porphyry	0.282 499–0.282 592	-7.3 to -3.7	1 271–1 470	Ai (2013)
	0.282 480–0.282 580	-7.2 to -3.6	1 437–1 666	Yuan et al. (2014)
Syenogranite	0.281 404–0.283 320	-10.2 to 2.87	1 025–1 850	This study

from other granite types in the Huangshaping Deposit (Table 8). On the other hand, the relatively lower $^{176}Hf/^{177}Hf$ ratios and negative $\varepsilon_{Hf}(t)$ values of spots No. 5 and No. 6 (inherited zircons) imply partial melting of a crustal source; and their old T_{DM1} (2 188–2 550 Ma) suggest that the source region of the syenogranite magma could probably the Paleoproterozoic or even older basement rocks. Thus, it can be concluded that the syenogranite was derived from the partial melting of Proterozoic basement rocks, with significant input of mantle materials.

4.3 Evolution, Classification and Tectonic Setting of Huangshaping Granites

Different types of granites produced by frequent magmatism at the Huangshaping Deposit resulted from multi-stage magmas (Yuan et al., 2014; Wang et al., 2011; Liu et al., 2009; Tong et al., 2000; Zhong, 1996). The chondrite-normalized REE patterns and the primitive mantle-normalized multi-element patterns of the syenogranite are quite similar to those of quartz porphyry and granophyre, indicating a similar magma evolutionary process among the three granites. In contrast, distinguished patterns are shown for the granite porphyry, suggesting the highest evolved degree for its magma (Li et al., 2014a, b). The potential location of the syenogranite is just beneath the granophyre (Fig. 2b), also indicating the closest relationship between the granophyre and the syenogranite in space. Geochemically, the trace elements such as Ba, Sr and Nb appear only in silicate minerals thus can apparently indicate the evolution of granitic magma. The average compositions of Ba (9.92 ppm) and Sr (17.2 ppm) in syenogranite are close to those in granite porphyry (7.24 ppm and 13.54 ppm, respectively) whereas less than

those in quartz porphyry (61.42 ppm and 47.07 ppm, respectively) and those in granophyre of (46.91 ppm and 44.47 ppm) (Table 2). In contrast, the average content of Rb in the syenogranite (463.8 ppm) is close to that of quartz porphyry (510.56 ppm) and granophyre (425 ppm) but is quite different from that of granite porphyry (973.78 ppm). The average Rb/Sr ratios are 10.85 for quartz porphyry, 9.56 for granophyre, 71.89 for granite porphyry and 33.36 for syenogranite, demonstrating that the granite porphyry experienced the strongest fractional crystallization, followed by syenogranite, quartz porphyry and then granophyre. All of these evidences fully proved that the evolutionary sequence is as follows: quartz porphyry→granophyre→syenogranite→granite porphyry. Therefore, we can infer that the syenogranite is a transitional magmatic phase between the granophyre and the granite porphyry.

The Huangshaping granites have been recognized as S-type granites or transitional type between S- and I-type for a long time (Liu et al., 2009; Yao et al., 2005; Zhong, 1996; Tong, 1986). However recently, Quan et al. (2012) divided these ore-forming related granites into the strong peraluminous A-type range and Li et al. (2014b) proposed that the quartz porphyry and granophyre can be classified as A_1-type alkaline granites whereas the granite porphyry is considered to be A_2-type aluminous granite. Similarly in this study, the syenogranite can be also classified as A-type granite (Figs. 9a–9d). Moreover, the syenogranite samples fall into the A_1 field (similar to the quartz porphyry and granophyre)

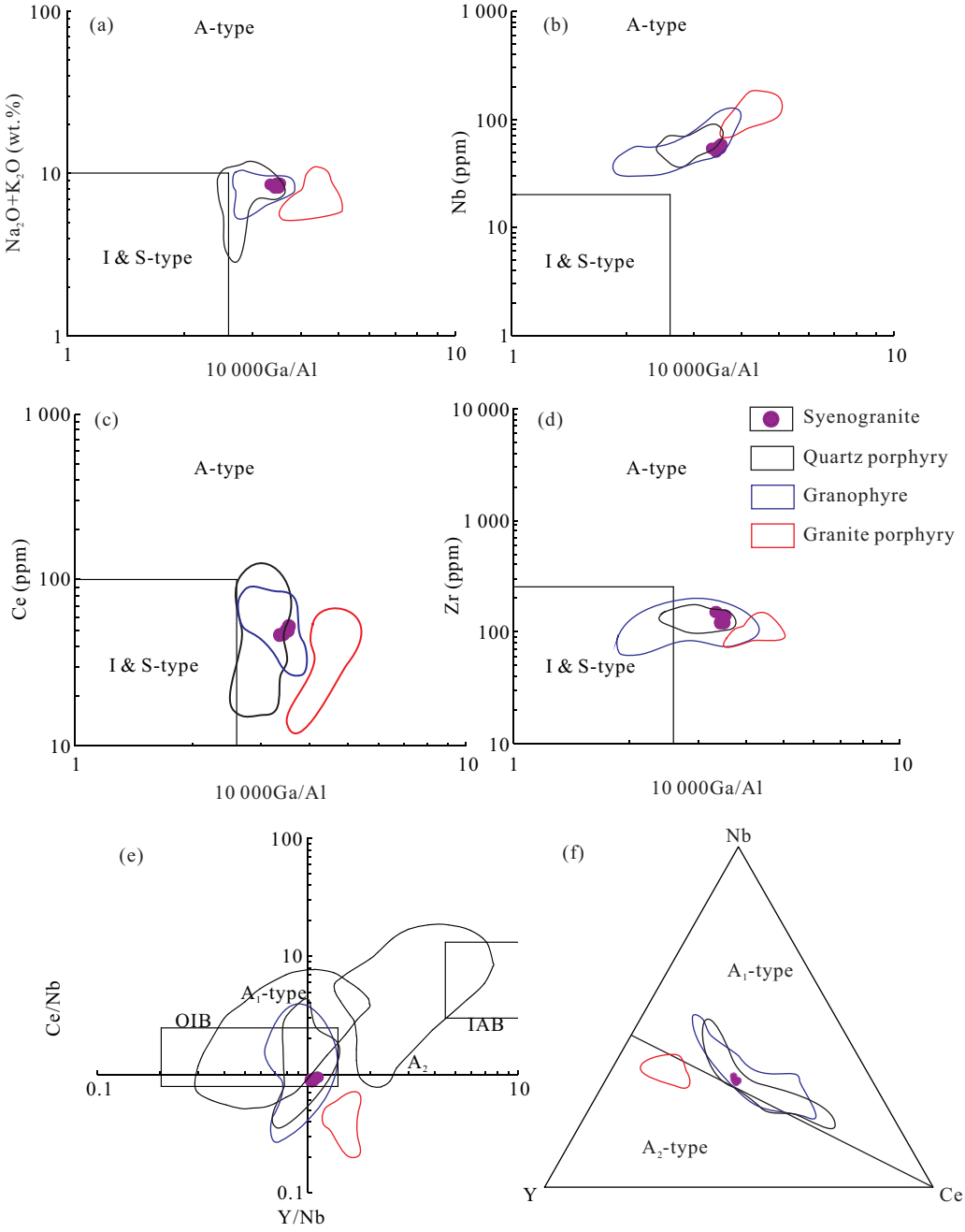

Figure 9. Geochemical classification for the A-type granites in the Huangshaping Deposit. (a) 10 000Ga/Al vs. Na_2O+K_2O diagram; (b) 10 000Ga/Al vs. Nb diagram; (c) 10 000Ga/Al vs. Ce diagram; (d) 10 000Ga/Al vs. Zr diagram; (e) Y/Nb vs. Ce/Nb diagram; (f) Nb-Y-Ce diagram; (a)–(d) after Whalen et al. (1987); (e) and (f) after Eby (1992).

whereas the granite porphyry plots in the A_2 field (Figs. 9e–9f). Moreover, the Huangshaping granite samples mainly fall into the "within-plate granite" field on the tectonic discrimination diagrams (Figs. 10a, 10b), overlapping with each other on the patterns except for the granite porphyry. Previous studies believed that A_1-type alkaline or peralkaline granites were mostly formed in within-plate anorogenic tectonic environment (Zhang et al., 2017; Wu et al., 2002; Patiño Douce, 1997; Hong et al., 1996). As a transitional type between the granophyre and granite porphyry, the magma of syenogranite may be generated in an intra-continental rift setting during the large-scale continental extension process.

4.4 Syenogranite-Related Cu Mineralization

The relationship between variable magmatic rocks and distinct mineralization types in the Huangshaping Deposit has been discussed since 1980s (He et al., 2010; Zhong, 1996; Tong, 1986). Some studies suggested that the granite porphyry provided the most ore-forming materials and energy for the mineralization (Zhu et al., 2012; Tong, 1986). In other opinions, the primary ore-forming materials were derived from the granophyre and supplemented by the granite porphyry (Zhong, 1996). Recently, it is believed that the Cu, Pb, Zn mineralization is intimately associated with the quartz porphyry whereas the W-Sn polymetallic mineralization is closely related to the granite porphyry (Liu et al., 2009). Afterwards, Lei et al. (2010) pointed out that the generation of W-Sn-Mo-Bi skarn-type ores are both associated with quartz porphyry and granite porphyry. Li et al. (2014b) reported that the quartz porphyry is weakly mineralized by the porphyry type Cu; the granophyre is related to the vein-type Pb-Zn mineralization; and the granite porphyry is closely associated with the skarn type W-Sn-Mo-Fe mineralization. However, a distinct perspective has been proposed in a most recent study (Ding et al., 2016a): significant amount of base metals (Pb and Zn) and S were extracted from basement material beneath southern Hunan whereas granitoids merely provided heat and fluid during the ore-forming process, except for the W-Sn mineralization which is still considered to be associated with granite porphyry.

The Jurassic granites were formed in the extensional environment and have experienced a stronger differentiation and evolution process (Li et al., 2018; Zhu et al., 2009; Bai et al., 2007; Wang et al., 2007; Zhou et al., 2006; Hua et al., 2005). The A_1-type granites in the Huangshaping Deposit, which include quartz porphyry, granophyre and the newly found syenogranite, are more or less associated with the Cu mineralization. The rapid extension of the crust may result in the deposition of deeply sourced Cu in a low-pressure environment. Partial melting of the lower crust which experienced intense mantle-crust interaction could produce A_1-type alkaline magmas as well as leach a large amount of Cu from the mantle, forming the Cu-dominated ore bodies in the earlier period of the Huangshaping Deposit. It is commonly approved that the early Jurassic syenite magmas in South China were closely associated with asthenospheric mantle under an intra-continental extension setting (Bai et al., 2015; Liu et al., 2013). Granitic magmas that underwent crust-mantle interaction are likely to result in Cu mineralization. This is consistent with our Hf data of the syenogranite, and we can infer that the participation of mantle material is a favorable factor for Cu mineralization.

On the other hand, the syenogranites also possess some similar geochemical characteristics to the granite porphyry. They contain more incompatible elements, volatile components, higher Rb/Sr ratios, lower Eu/Eu* values and higher alkalinity compared to quartz porphyry and granophyre in the Huangshaping Deposit. For the W-Sn polymetallic mineralization, the ore-forming ability and specialization of related granites depend on the contents of mineralizing elements, volatiles and heat producing elements (such as U, Th and other radioactive elements), oxidative statuses and Ph values (Bai et al., 2007). In contrast to other granites, the concentrations of U and Th in syenogranite samples are similar to those in granite porphyry whereas higher than those in quartz porphyry and granophyre. The average Rb/Sr and Eu/Eu* ratios also show a downward trend from granite porphyry and syenogranite to quartz porphyry and granophyre (Table 2). Therefore, the syenogranite possesses a strong W-Sn mineralization ability theoretically. The Cu-mineralized syenogranite is geochemically a transitional phase between the granophyre and

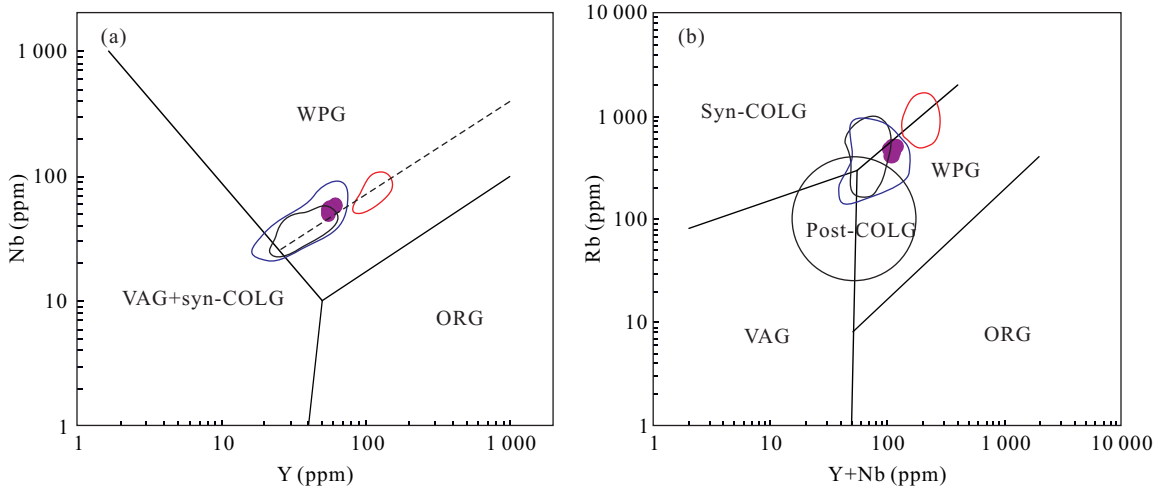

Figure 10. Discriminate diagrams of tectonic settings for the Huangshaping granites (after Pearce, 1996). (a) Y vs. Nb diagram and (b) Y+Nb vs. Rb diagram. WPG. Within plate granites; VAG. volcanic arc granites; ORG. ocean ridge granites; syn-COLG and post-COLG. syn- and post-collision granites.

the granite porphyry, indicating that the syenogranite may have not only contributed to the deep Cu ore formation but also played a role of "vanguard" for the later W-Sn polymetallic mineralization in the Huangshaping Deposit. Many scholars pointed out that mantle-derived material have played an important role during the emplacement of Jurassic granites (Zhou et al., 2016), and the crust-mantle interaction may have played an important role in the formation of world class W-Sn polymetallic deposits in the Nanling region (Chen et al., 2016; Zhu et al., 2009; Jiang et al., 2008; Li et al., 2006; Zhao et al., 2001).

5 CONCLUSIONS

(1) The newly found fine-grained biotite syenogranite in the Huangshaping Deposit is a transitional phase between the granophyre and the granite porphyry, belonging to A_1-type alkaline granite and forming under an intraplate extensional setting.

(2) The U-Pb dating of magmatic and hydrothermal zircons in the syenogranite yielded the $^{206}Pb/^{238}U$ concordant ages of 156.5±1.8 and 154.4±2.9 Ma, representing the crystallization and related Cu mineralization ages, respectively. The syenogranite magma may be derived from Paleoproterozoic basement (lower crust) and experienced substantial mantle-crust interaction.

(3) The syenogranite may have not only contributed to the deep Cu mineralization but also induced the later W-Sn polymetallic ore formation in the Huangshaping Deposit.

ACKNOWLEDGMENTS

This work was co-financed by the National Natural Science Foundation of China (Nos. 41502067, 41672074) and the Fundamental Research Funds for the Central Universities, China University of Geosciences (Wuhan) (No. CUG150612). The authors thank researcher Li Liu for his technical assistance in LA-ICP-MS analysis. The final publication is available at Springer via https://doi.org/10.1007/s12583-017-0974-7.

REFERENCES CITED

Ai, H., 2013. Zircon U-Pb Geochronology and Hf Isotopic Compositions of Ore-Related Granites from Huangshaping Polymetallic Deposit of Hunan Province. *Mineral Deposits*, 32(3): 545–563. https://doi.org/10.16111/j.0258-7106.2013.03.006 (in Chinese with English Abstract)

Andersen, T., 2002. Correction of Common Lead in U-Pb Analyses that do not Report ^{204}Pb. *Chemical Geology*, 192(1/2): 59–79. https://doi.org/10.1016/s0009-2541(02)00195-x

Bai, D. Y., Jia, B. H., Ma, T. Q., et al., 2007. Relationship of Petro-Geochemical Characteristics to Metallogenic Capacity Differences between Indosinian and Early Yanshanian Granites in Southeastern Hunan. *Acta Petrologica et Mineralogica*, 26(5): 387–398 (in Chinese with English Abstract)

Bai, Z. J., Zhu, W. G., Zhong, H., et al., 2015. Petrogenesis and Tectonic Implications of the Early Jurassic Fe-Ti Oxide-Bearing Xialan Mafic Intrusion in SE China: Constraints from Zircon Hf-O Isotopes, Mineral Compositions and Whole-Rock Geochemistry. *Lithos*, 212–215: 59–73. https://doi.org/10.13039/501100001809

Cai, M. H., Han, F. B., He, L. Q., et al., 2008. He, Ar Isotope Characteristics and Rb-Sr Dating of the Xintianling Skarn Scheelite Deposit in Southern Hunan, China. *Acta Geoscientica Sinica*, 29(2): 167–173 (in Chinese with English Abstract)

Chen, L., Liu, Y. S., Hu, Z. C., et al., 2011. Accurate Determinations of Fifty-Four Major and Trace Elements in Carbonate by LA-ICP-MS Using Normalization Strategy of Bulk Components as 100%. *Chemical Geology*, 284(3/4): 283–295. https://doi.org/10.1016/j.chemgeo.2011.03.007

Chen, R. H., Deng, B. H., Gong, S. Q., et al., 2013. Geological Characteristics and Metallogenic Regularity of Huangshaping Pb-Zn Polymetallic Deposit, Southern Hunan Province. *Geology and Mineral Resources of South China*, 29(1): 46–53. https://doi.org/10.3969/j.issn.1007-3701.2013.01.007 (in Chinese with English Abstract)

Chen, Y. X., Li, H., Sun, W. D., et al., 2016. Generation of Late Mesozoic Qianlishan A_2-type granite in Nanling Range, South China: Implications for Shizhuyuan W-Sn Mineralization and Tectonic Evolution. *Lithos*, 266: 435–452. https://10.1016/j.lithos.2016.10.010

Ding, T., Ma, D. S., Lu, J. J., et al., 2016a. S, Pb, and Sr Isotope Geochemistry and Genesis of Pb-Zn Mineralization in the Huangshaping Polymetallic Ore Deposit of Southern Hunan Province, China. *Ore Geology Reviews*, 77: 117–132. https://doi.org/10.13039/501100001809

Ding, T., Ma, D. S., Lu, J. J., et al., 2016b. Petrogenesis of Late Jurassic Granitoids and Relationship to Polymetallic Deposits in Southern China: The Huangshaping Example. *International Geology Review*, 58(13): 1646–1672. https://doi.org/10.13039/501100001809

Eby, G. N., 1992. Chemical Subdivision of the A-Type Granitoids: Petrogenetic and Tectonic Implications. *Geology*, 20(7): 641–644. https://doi.org/10.1130/0091-7613(1992)020<0641:csotat>2.3.co;2

Frost, B. R., Barnes, C. G., Collins, W. J., et al., 2001. A Geochemical Classification for Granitic Rocks. *Journal of Petrology*, 42(11): 2033–2048. https://doi.org/10.1093/petrology/42.11.2033

Fu, B., Mernagh, T. P., Kita, N. T., et al., 2009. Distinguishing Magmatic Zircon from Hydrothermal Zircon: A Case Study from the Gidginbung High-Sulphidation Au-Ag-(Cu) Deposit, SE Australia. *Chemical Geology*, 259(3/4): 131–142. https://doi.org/10.1016/j.chemgeo.2008.10.035

Geisler, T., Rashwan, A. A., Rahn, M. K. W., et al., 2003. Low-Temperature Hydrothermal Alteration of Natural Metamict Zircons from the Eastern Desert, Egypt. *Mineralogical Magazine*, 67(3): 485–508. https://doi.org/10.1180/0026461036730112

He, H. Q., Wang, J. C., Jiang, Y. C., 2010. Preliminary Analysis on the Geological Characteristics and Genesis of Fe-W-Mo-Bi (-Sn) Polymetallic Deposit in the Southern Huangshaping Lead-Zinc Mine District, Hunan. *Mineral Exploration*, 1(4): 323–333 (in Chinese with English Abstract)

Hong, D. W., Wang, S. G., Han, B. F., et al., 1996. Post-Orogenic Alkaline Granites from China and Comparisons with Anorogenic Alkaline Granites Elsewhere. *Journal of Southeast Asian Earth Sciences*, 13(1): 13–27. https://doi.org/10.1016/0743-9547(96)00002-5

Hoskin, P. W. O., 2005. Trace-Element Composition of Hydrothermal Zircon and the Alteration of Hadean Zircon from the Jack Hills, Australia. *Geochimica et Cosmochimica Acta*, 69(3): 637–648. https://doi.org/10.1016/j.gca.2004.07.006

Hou, K. J., Li, Y. H., Zou, T. R., et al., 2007. Laser Ablation-MC-ICP-MS Technique for Hf Isotope Microanalysis of Zircon and Its Geological Applications. *Acta Petrologica Sinica*, 23(10): 2595–2604 (in Chinese with English Abstract)

Hu, F. F., Fan, H. R., Yang, J. H., et al., 2004. Mineralizing Age of the Rushan Lode Gold Deposit in the Jiaodong Peninsula: SHRIMP U-Pb Dating on Hydrothermal Zircon. *Chinese Science Bulletin*, 49(15): 1629–1636. https://doi.org/10.1007/bf03184134

Hu, Z. C., Gao, S., Liu, Y. S., et al., 2008. Signal Enhancement in Laser

Ablation ICP-MS by Addition of Nitrogen in the Central Channel Gas. *Journal of Analytical Atomic Spectrometry*, 23(8): 1093–1101. https://doi.org/10.1039/b804760j

Hua, R. M., Chen, P. R., Zhang, W. L., et al., 2005. Metallogenesis Related to Mesozoic Granitoids in the Nanling Range, South China and Their Geodynamic Settings. *Acta Geologica Sinica—English Edition*, 79(6): 810–820. https://doi.org/10.1111/j.1755-6724.2005.tb00936.x

Jackson, S. E., Pearson, N. J., Griffin, W. L., et al., 2004. The Application of Laser Ablation-Inductively Coupled Plasma-Mass Spectrometry to *in situ* U-Pb Zircon Geochronology. *Chemical Geology*, 211(1/2): 47–69. https://doi.org/10.1016/j.chemgeo.2004.06.017

Jiang, S. Y., Zhao. K. D., Jiang, Y. H., et al., 2008. Characteristics and Genesis of Mesozoic A-Type Granites and Associated Mineral Deposits in the Southern Hunan and Northern Guangxi Provinces along the Shi-Hang Belt, South China. *Geological Journal of China Universities*, 14(4): 96–509. https://doi.org/10.16108/j.issn1006-7493.2008.04.011 (in Chinese with English Abstract)

Lai, S. H., 2014. Research on Mineralization of the Xianghualing Tin Polymetallic Deposit, Hunan Province, China: [Dissertation]. China University of Geosciences, Beijing. 42–60 (in Chinese with English Abstract)

Le Bas, M. J., Le Maitre, R. W., Streckeisen, A., et al., 1986. A Chemical Classification of Volcanic Rocks Based on the Total Alkali-Silica Diagram. *Journal of Petrology*, 27(3): 745–750. https://doi.org/10.1093/petrology/27.3.745

Le Maitre, R. W., 1989. A Classification of Igneous Rocks and Glossary of Terms: Recommendations of the IUGS Commission on the Systematics of Igneous Rocks. Blackwell, Oxford. 1–34

Lei, Z. H., Chen, F. W., Chen, Z. H., et al., 2010. Petrogenetic and Metallogenic Age Determination of the Huangshaping Lead-Zinc Polymetallic Deposit and Its Geological Significance. *Acta Geoscientia Sinica*, 31(4): 532–540 (in Chinese with English Abstract)

Li, C. M., 2009. A Review on the Minerageny and *in situ* Microanalytical Dating Techniques of Zircons. *Geological Survey and Research*, 33(3): 161–174 (in Chinese with English Abstract)

Li, H. Q., Lu, Y. F., Wang, D. H., et al., 2006. Dating of the Rock-Forming and Ore-Forming Ages and Their Geological Significances in the Furong Ore-Field, Qitian Mountain, Hunan. *Geological Review*, 52(1): 113–121. https://doi.org/10.16509/j.georeview.2006.01.017 (in Chinese with English Abstract)

Li, H. Y., Mao, J. W., Sun, Y. L., et al., 1996. Re-Os Isotopic Chronology of Molybdenites in the Shizhuyuan Polymetallic Tungsten Deposit, Southern Hunan. *Geological Review*, 42(3): 261–267. https://doi.org/10.16509/j.georeview.1996.03.011 (in Chinese with English Abstract)

Li, H., Palinkaš, L. A., Watanabe, K., et al., 2018. Petrogenesis of Jurassic A-Type Granites Associated with Cu-Mo and W-Sn Deposits in the Central Nanling Region, South China: Relation to Mantle Upwelling and Intra-Continental Extension. *Ore Geology Reviews*, 92: 449–462. https://doi.org/ 10.1016/j.oregeorev.2017.11.029

Li, H., Sun, H. S., Wu, J. H., et al., 2017a. Re-Os and U-Pb Geochronology of the Shazigou Mo Polymetallic Ore Field, Inner Mongolia: Implications for Permian–Triassic Mineralization at the Northern Margin of the North China Craton. *Ore Geology Reviews*, 83: 287–299. https://doi.org/10.13039/501100001809

Li, H., Yonezu, K., Watanabe, K., et al., 2017b. Fluid Origin and Migration of the Huangshaping W-Mo Polymetallic Deposit, South China: Geochemistry and $^{40}Ar/^{39}Ar$ Geochronology of Hydrothermal K-Feldspars. *Ore Geology Reviews*, 86: 117–129. https://doi.org/10.13039/501100001809

Li, H., Watanabe, K., Yonezu, K., 2014a. Zircon Morphology, Geochronology and Trace Element Geochemistry of the Granites from the Huangshaping Polymetallic Deposit, South China: Implications for the Magmatic Evolution and Mineralization Processes. *Ore Geology Reviews*, 60: 14–35. https://doi.org/10.1016/j.oregeorev.2013.12.009

Li, H., Watanabe, K., Yonezu, K., 2014b. Geochemistry of A-Type Granites in the Huangshaping Polymetallic Deposit (South Hunan, China): Implications for Granite Evolution and Associated Mineralization. *Journal of Asian Earth Sciences*, 88: 149–167. https://doi.org/10.1016/j.jseaes.2014.03.004

Li, J. D., Bai, D. Y., Wu, G. Y., et al., 2005. Zircon SHRIMP Dating of the Qitianling Granite, Chenzhou, Southern Hunan, and Its Geological Significance. *Geological Bulletin of China*, 24(5): 411–414 (in Chinese with English Abstract)

Li, S. T., Wang, J. B., Zhu, X. Y., et al., 2011a. Chronological Characteristics of the Yaogangxian Composite Pluton in Hunan Province. *Geology and Exploration*, 47(2): 143–150 (in Chinese with English Abstract)

Li, S. T., Wang, J. B., Zhu, X. Y., et al., 2011b. Re-Os Dating of Molybdenite and Sulfur Isotope Analysis of the Yaogangxiang Tungsten Polymetallic Deposits in Hunan Province and Their Geological Significance. *Geoscience*, 25(2): 228–235 (in Chinese with English Abstract)

Li, X. H., Liu, D. Y., Sun, M., et al., 2004. Precise Sm-Nd and U-Pb Isotopic Dating of the Supergiant Shizhuyuan Polymetallic Deposit and Its Host Granite, SE China. *Geological Magazine*, 141(2): 225–231. https://doi.org/10.1017/s0016756803008823

Liu, X. F., Yuan, S. D., Wu, S. H., 2012. Re-Os Dating of the Molybdenite from the Jinchuantang Tin-Bismuth Deposit in Hunan Province and Its Geological Significance. *Acta Petrologica Sinica*, 28(1): 39–51 (in Chinese with English Abstract)

Liu, X., Liu, W. H., Xi, C. Z., et al., 2009. Geochemical Characteristics of Magmatic Rocks of Huangshaping Lead-Zinc Deposit in Hunan, China. *Contributions to Geology and Mineral Resources Research*, 24(3): 198–204 (in Chinese with English Abstract)

Liu, Y. S., Hu, Z. C., Gao, S., et al., 2008. *In situ* Analysis of Major and Trace Elements of Anhydrous Minerals by LA-ICP-MS without Applying an Internal Standard. *Chemical Geology*, 257(1/2): 34–43. https://doi.org/10.1016/j.chemgeo.2008.08.004

Liu, Y. S., Hu, Z. C., Zong, K. Q., et al., 2010. Reappraisement and Refinement of Zircon U-Pb Isotope and Trace Element Analyses by LA-ICP-MS. *Chinese Science Bulletin*, 55(15): 1535–1546. https://doi.org/10.1007/s11434-010-3052-4

Liu, Y., Cheng, Q. M., Xia, Q. L., et al., 2013. Application of Singularity Analysis for Mineral Potential Identification Using Geochemical Data—A Case Study: Nanling W-Sn-Mo Polymetallic Metallogenic Belt, South China. *Journal of Geochemical Exploration*, 134: 61–72. https://doi.org/10.1016/j.gexplo.2013.08.006

Lu, Y. F., Ma, L. Y., Qu, W. J., et al., 2006. U-Pb and Re-Os Isotope Geochronology of Baoshan Cu-Mo Polymetallic Ore Deposit in Hunan Province. *Acta Petrologica Sinica*, 22(10): 2483–2492 (in Chinese with English Abstract)

Ludwig, K. R., 2003. ISOPLOT/Ex, Version 3, A Geochronological Toolkit for Microsoft Excel. Berkeley Geochronology Center, Berkeley. 1–39

Ma, L. Y., Lu, Y. F., Qu, W. J., et al., 2007. Re-Os Isotopic Chronology of Molybdenites in Huangshaping Lead-Zinc Deposit, Southeast Hunan, and Its Geological Implications. *Mineral Deposits*, 26(4): 425–431 (in Chinese with English Abstract)

Mao, J. W., Cheng, Y. B., Chen, M. H., et al., 2013. Major Types and Time-Space Distribution of Mesozoic Ore Deposits in South China

and Their Geodynamic Settings. *Mineralium Deposita*, 48(3): 267–294. https://doi.org/10.1007/s00126-012-0446-z

Mao, J. W., Li, H. Y., Pei, R. F., 1995. Nd-Sr Isotopic and Petrogenetic Studies of the Qianlishan Granite Stock, Hunan Province. *Mineral Deposits*, 14(3): 235–242 (in Chinese with English Abstract)

Mao, J. W., Li, X. F., Lehmann, B., et al., 2004. ^{40}Ar-^{39}Ar Dating of Tin Ores and Related Granite in Furong Tin Orefield Hunan Province, and Its Geodynamic Significance. *Mineral Deposits*, 23(2): 164–175. https://doi.org/10.16111/j.0258-7106.2004.02.005 (in Chinese with English Abstract)

Mao, J. W., Xie, G. Q., Guo, C. L., et al., 2007. Large-Scale Tungsten-Tin Mineralization in the Nanling Region, South China: Metallogenic Ages and Corresponding Geodynamic Processes. *Acta Petrologica Sinica*, 23(10): 2329–2338 (in Chinese with English Abstract)

Mi, J. R., 2016. The Study of Genetic Difference between Cu and W Deposits in Southern Hunan-Take the Baoshan and Huangshaping Deposits as an Example: [Dissertation]. China University of Geosciences, Beijing. 39–41 (in Chinese with English Abstract)

Morel, M. L. A., Nebel, O., Nebel-Jacobsen, Y. J., et al., 2008. Hafnium Isotope Characterization of the GJ-1 Zircon Reference Material by Solution and Laser-Ablation MC-ICPMS. *Chemical Geology*, 255(1/2): 231–235. https://doi.org/10.1016/j.chemgeo.2008.06.040

Patiño Douce, A. E., 1997. Generation of Metaluminous A-Type Granites by Low-Pressure Melting of Calc-Alkaline Granitoids. *Geology*, 25(8): 743–746. https://doi.org/10.1130/0091-7613(1997)025<0743:gomatg>2.3.co;2

Pearce, J. A., 1996. Sources and Settings of Granitic Rocks. *Episodes*, 19(4): 120–125

Peng, J. T., Hu, R. Z., Bi, X. W., et al., 2007. ^{40}Ar/^{39}Ar Isotopic Dating of Tin Mineralization in Furong Deposit of Hunan Province and Its Geological Significance. *Mineral Deposits*, 26(3): 237–248. https://doi.org/10.16111/j.0258-7106.2007.03.001 (in Chinese with English Abstract)

Peng, J. T., Zhou, M. F., Hu, R. Z., et al., 2006. Precise Molybdenite Re-Os and Mica Ar-Ar Dating of the Mesozoic Yaogangxian Tungsten Deposit, Central Nanling District, South China. *Mineralium Deposita*, 41(7): 661–669. https://doi.org/10.1007/s00126-006-0084-4

Qi, F. Y., Zhang, Z., Zhu, X. Y., et al., 2012. Skarn Geochemistry of the Huangshaping W-Mo Polymetallic Deposit in Hunan and Its Geological Significance. *Geology in China*, 39(2): 338–348 (in Chinese with English Abstract)

Quan, T. J., Kong, H., Wang, G., et al., 2012. Petrogenesis of the Granites in the Huangshaping Area: Constrains from Petrochemistry, Zircon U-Pb Chronology and Hf Isotope. *Geotectonica et Metallogenica*, 36(4): 597–606. https://doi.org/10.16539/j.ddgzyckx.2012.04.016 (in Chinese with English Abstract)

Sun, S. S., McDonough, W. F., 1989. Chemical and Isotopic Systematics of Oceanic Basalts: Implications for Mantle Composition and Processes. *Geological Society*, *London*, *Special Publications*, 42(1): 313–345. https://doi.org/10.1144/gsl.sp.1989.042.01.19

Tong, Q. M., 1986. The Characteristics of Metallogeny of the Huangshaping Lead-Zinc Ore Deposit of Southern Hunan. *Geological Review*, 32(6): 565–577 (in Chinese with English Abstract)

Tong, Q. M., Li, R. Q., Zhang, J. X., 2000. The Characteristics of Magmatic Rocks along the Chenzhou-Linwu Deep-Seated Fault. *Geology and Mineral Resources of South China*, (3): 8–16 (in Chinese with English Abstract)

Wang, L. F., Jiang, Y. C., Wang, L. F., et al., 2011. Geological Characteristics and Prospecting Direction of the Copper Deposit of the Huangshaping Ore Field in Hunan. *Mineral Exploration*, 2(3): 226–231 (in Chinese with English Abstract)

Wang, Y. J., Fan, W. M., Sun, M., et al., 2007. Geochronological, Geochemical and Geothermal Constraints on Petrogenesis of the Indosinian Peraluminous Granites in the South China Block: A Case Study in the Hunan Province. *Lithos*, 96(3/4): 475–502. https://doi.org/10.1016/j.lithos.2006.11.010

Wang, Z. Q., Chen, B., Ma, X. H., 2014. *In situ* LA-ICP-MS U-Pb Age and Geochemical Data of Cassiterite of the Furong Tin Deposit, the Nanling Range: Implications for the Origin and Evolution of the Ore-Forming Fluid. *Chinese Science Bulletin*, 59(25): 2505–2519 (in Chinese)

Whalen, J. B., Currie, K. L., Chappell, B. W., 1987. A-Type Granites: Geochemical Characteristics, Discrimination and Petrogenesis. *Contributions to Mineralogy and Petrology*, 95(4): 407–419. https://doi.org/10.1007/bf00402202

Wheller, G. E., Varne, R., Foden, J. D., et al., 1987. Geochemistry of Quaternary Volcanism in the Sunda-Banda Arc, Indonesia, and Three-Component Genesis of Island-Arc Basaltic Magmas. *Journal of Volcanology and Geothermal Research*, 32(1/2/3): 137–160. https://doi.org/10.1016/0377-0273(87)90041-2

Wiedenbeck, M., Hanchar, J. M., Peck, W. H., et al., 2004. Further Characterisation of the 91500 Zircon Crystal. *Geostandards and Geoanalytical Research*, 28(1): 9–39. https://doi.org/10.1111/j.1751-908x.2004.tb01041.x

Wu, F. Y., Sun, D. Y., Li, H. M., et al., 2002. A-Type Granites in Northeastern China: Age and Geochemical Constraints on Their Petrogenesis. *Chemical Geology*, 187(1/2): 143–173. https://doi.org/10.1016/s0009-2541(02)00018-9

Wu, F. Y., Yang, Y. H., Xie, L. W., et al., 2006. Hf Isotopic Compositions of the Standard Zircons and Baddeleyites Used in U-Pb Geochronology. *Chemical Geology*, 234(1/2): 105–126. https://doi.org/10.1016/j.chemgeo.2006.05.003

Xiao, H. Q., Zhao, K. D., Jiang, S. Y., et al., 2003. Lead Isotope Geochemistry and Ore-Forming Age of Jinchuantang Sn-Bi Deposit in Dongpo Ore Field, Hunan Province. *Mineral Deposits*, 22(3): 264–270. https://doi.org/10.16111/j.0258-7106.2003.03.008 (in Chinese with English Abstract)

Xu, Y. M., Gong, S. Q., Jiang, Y. C., et al., 2007. Hunan Huangshaping Lead Zinc Mine of the Deep Analysis of the Prospects for Lead Zinc Mine Resources. *Geology and Prospecting*, 43(1): 38–43 (in Chinese with English Abstract)

Yao, J. M., Hua, R. M., Lin, J. F., 2005. Zircon LA-ICPMS U-Pb Dating and Geochemical Characteristics of Huangshaping Granite in Southeast Hunan Province, China. *Acta Petrologica Sinica*, 21(3): 688–696 (in Chinese with English Abstract)

Yao, J. M., Hua, R. M., Lin, J. F., 2006. REE, Pb-S Isotope Geochemistry, and Rb-Sr Isochron Age of Pyrites in the Baoshan Deposit, South Hunan Province, China. *Acta Geologica Sinica*, 80(7): 1045–1054 (in Chinese with English Abstract)

Yao, J. M., Hua, R. M., Qu, W. J., et al., 2007. Re-Os Isotope Dating of Molybdenites in the Huangshaping Pb-Zn-W-Mo Polymetallic Deposit, Hunan Province, South China and Its Geological Significance. *Science in China Series D*: *Earth Sciences*, 50(4): 519–526. https://doi.org/10.1007/s11430-007-2052-y

Yuan, S. D., Peng, J. T., Hu, R. Z., et al., 2008. A Precise U-Pb Age on Cassiterite from the Xianghualing Tin-Polymetallic Deposit (Hunan, South China). *Mineralium Deposita*, 43(4): 375–382. https://doi.org/10.1007/s00126-007-0166-y

Yuan, S. D., Peng, J. T., Shen, N. P., et al., 2007. ^{40}Ar-^{39}Ar Isotopic Dating of the Xianghualing Sn-Polymetallic Orefield in Southern Hunan, China and Its Geological Implications. *Acta Geologica Sinica—English Edition*, 81(2): 278–286. https://doi.org/10.1111/j.1755-6724.2007.tb00951.x

Yuan, S. D., Zhang, D. L., Shuang, Y., et al., 2012. Re-Os Dating of Molybdenite from the Xintianling Giant Tungsten-Molybdenum Deposit in Southern Hunan Province, China and Its Geological Implications. *Acta Petrologica Sinica*, 28(1): 27–38 (in Chinese with English Abstract)

Yuan, Y. B., Yuan, S. D., Chen, C. J., et al., 2014. Zircon U-Pb Ages and Hf Isotopes of the Granitoids in the Huangshaping Mining Area and Their Geological Significance. *Acta Petrologica Sinica*, 30(1): 64–78 (in Chinese with English Abstract)

Zeng, Z. X., 2001. Geological Characteristics and Genesis of the Copper Deposit of the Huangshaping Ore Field. *Hunan Nonferrous Metals*, 17(3): 8–9, 13 (in Chinese with English Abstract)

Zhang, X. B., Wang, K. Y., Wang, C. Y., et al., 2017. Age, Genesis, and Tectonic Setting of the Mo-W Mineralized Dongshanwan Granite Porphyry from the Xilamulun Metallogenic Belt, NE China. *Journal of Earth Science*, 28(3): 433–446. https://doi.org/10.1007/s12583-016-0934-1

Zhang, X. W., Xiang, H., Zhong, Z. Q., et al., 2009. U-Pb Dating and Trace Elements Composition of Hydrothermal Zircons from Jianfengling Granite, Hainan: Restriction on the Age of Hydrothermal Event and Mineralization of Baolun Gold Deposit. *Earth Science—Journal of China University of Geosciences*, 34(6): 921–930 (in Chinese with English Abstract)

Zhao, Z. H., Bao, Z. W., Zhang, B. Y., et al., 2001. Crust-Mantle Interaction and Its Contribution to the Shizhuyuan Superlarge Tungsten Polymetallic Mineralization. *Science in China Series D*: *Earth Sciences*, 44(3): 266–276. https://doi.org/10.1007/BF02882261

Zhong, Z. C., 1996. Magma Rocks and Their Ore-Controlling Characteristics in the Huangshaping Mining Area. *Mineral Resources and Geology*, 10(6): 400–405. https://doi.org/10.16111/j.0258-7106.2010.s1.187 (in Chinese with English Abstract)

Zhou, X. M., Li, W. X., 2000. Origin of Late Mesozoic Igneous Rocks in Southeastern China: Implications for Lithosphere Subduction and Underplating of Mafic Magmas. *Tectonophysics*, 326(3/4): 269–287. https://doi.org/10.1016/s0040-1951(00)00120-7

Zhou, X. M., Sun, T., Shen, W. Z., et al., 2006. Petrogenesis of Mesozoic Granitoids and Volcanic Rocks in South China: A Response to Tectonic Evolution. *Episodes*, 29(1): 26–33

Zhou, Z. M., Ma, C. Q., Xie, C. F., et al., 2016. Genesis of Highly Fractionated I-Type Granites from Fengshun Complex: Implications to Tectonic Evolutions of South China. *Journal of Earth Science*, 27(3): 444–460. https://doi.org/10.1007/s12583-016-0677-3

Zhu, J. C., Wang, R. C., Zhang, P. H., et al., 2009. Zircon U-Pb Geochronological Framework of Qitianling Granite Batholith, Middle Part of Nanling Range, South China. *Science in China Series D*: *Earth Sciences*, 50(4): 1279–1294. https://doi.org/10.1007/s11430-009-0154-4

Zhu, J. C., Chen, J., Wang, R. C., et al., 2008. Early Yanshanian Ne Trending Sn/W-Bearing A-Type Granites in the Western-Middle Part of the Nanling Mts Region. *Geological Journal of China Universities*, 14(4): 474–484. https://doi.org/10.16108/j.issn1006-7493.2008.04.010 (in Chinese with English Abstract)

Zhu, X. Y., Wang, J. B., Wang, Y. L., et al., 2012. Sulfur and Lead Isotope Constraints on Ore Formation of the Huangshaping W-Mo-Bi-Pb-Zn Polymetallic Ore Deposit, Hunan Province, South China. *Acta Petrologica Sinica*, 28(12): 3809–3822 (in Chinese with English Abstract)